



**POLITECNICO**  
MILANO 1863

SCUOLA DI INGEGNERIA INDUSTRIALE  
E DELL'INFORMAZIONE

# Fuel-optimal acquisition and control of a cartwheel formation in Earth Displaced Heliocentric Orbit

TESI DI LAUREA MAGISTRALE IN  
SPACE ENGINEERING - INGEGNERIA SPAZIALE

Author: **Stefano Marmorì**

Student ID: 963530

Advisor: Prof. Francesco Topputo

Co-advisors: Dr. Alessandro Morselli

Academic Year: 2022-23



# Abstract

In the last decades formation flying obtained such prolific results that ESA, in collaboration with NASA, decided to develop one of the most ambitious missions ever conceived: Laser Interferometer Space Antenna (LISA). The objective of the mission is to observe the entire universe in search of gravitational waves, detecting and measuring with high precision this obscure phenomenon. LISA assumes the so-called cartwheel formation, where three satellites uniformly distributed on a circumference, keep a rotating triangular configuration during operation in an Earth Displaced Heliocentric Orbit (EDHO). The uniqueness of LISA is due to the fact that just gravitational accelerations affect the spacecraft's motion, making previous studies on this formation valid only for this peculiar mission. The work aims to generalise the framework in which this type of cartwheel formation has been investigated up to now, focusing on two main objectives: the acquisition of the formation and the transfer of the fleet from Earth to the final heliocentric orbit. In a different dynamical environment, the satellites must maintain the correct reciprocal position to keep the stability, measured using geometrical parameters like arm length, arm length rate and corner angle, within the imposed requirements. The stabilization process is tackled by optimizing the initial conditions of the spacecraft starting from a Keplerian definition of the cartwheel configuration; this optimization is proposed for multiple type of formation with different initial displacement angles and arm lengths. Regarding the first phase, a single launch containing all the units is considered; this imposes a major challenge in the mediation process between the transfer and the science phase in which the inter-satellite distance pass from zero to 2.5 million km. This issue is addressed by developing two different strategies which aim directly at the final science orbits previously optimized. These results provide a more general view of the cartwheel formation flying in EDHO suggesting a possible optimization approach for the maintenance of the configuration and defining a fuel-optimal transfer design for future works.

**Keywords:** Cartwheel Formation Flying; Trajectory Design; Earth Displaced Heliocentric Orbits; Optimized Formation;



## Abstract in lingua italiana

Nelle ultime decadi le missioni in formazione hanno ottenuto risultati così positivi da portare l'ESA, in collaborazione con la NASA, a sviluppare una delle più ambiziose missioni mai concepite: LISA. L'obiettivo della missione è quello di osservare l'intero universo in cerca di onde gravitazionali, individuando e misurando con elevata precisione questo fenomeno. La configurazione assunta da LISA, chiamata 'cartwheel', è composta da tre satelliti distribuiti uniformemente su una circonferenza su cui la formazione ruota mantenendo una geometria triangolare durante le operazioni in EDHO. L'unicità di LISA è dovuta al fatto che solamente accelerazioni gravitazionali ne influenzano la dinamica, limitando la validità di precedenti studi a questa missione. La tesi punta a generalizzare il framework in cui questo tipo di configurazione a 'cartwheel' è stata investigata fino ad ora, concentrandosi su due maggiori obiettivi: la stabilità della formazione e il trasferimento della flotta dalla Terra fino all'orbita eliocentrica finale. Soggetti ad una diversa dinamica, i satelliti devono mantenere la corretta posizione reciproca per conservare la stabilità, misurata attraverso la lunghezza dei bracci, le velocità relative e l'angolo tra i bracci, entro i limiti richiesti. Il processo di stabilizzazione è affrontato ottimizzando le condizioni iniziali del satellite partendo da una definizione Kelperiana della configurazione. L'ottimizzazione viene proposta per vari tipi di geometria modificando l'angolo di spostamento iniziale e la lunghezza dei bracci. Per quanto riguarda la prima fase della missione viene considerato un singolo lancio contenente tutti e tre i satelliti; questo impone una maggiore sfida per il passaggio dal trasferimento alla fase scientifica in cui la distanza tra i satelliti passa da zero a 2.5 milioni di km. Questo problema viene trattato sviluppando due diverse strategie che puntano direttamente alle orbite scientifiche finali precedentemente ottimizzate. Questi risultati forniscono una visuale più generale sulla 'cartwheel' formation in EDHO suggerendo un possibile approccio di ottimizzazione per il suo mantenimento e trasferimento per lavori futuri.

**Parole chiave:** Formazione a Cartwheel; Design di Traiettoria; EDHO; Formazione Ottimizzata;



# Contents

|   |             |
|---|-------------|
| <b>Abstract</b>   | <b>i</b>    |
| <b>Abstract in lingua italiana</b>                        | <b>iii</b>  |
| <b>Contents</b>   | <b>v</b>    |
| <b>List of Figures</b>                                    | <b>vii</b>  |
| <b>List of Tables</b>                                     | <b>ix</b>   |
| <b>Acronyms</b>   | <b>xi</b>   |
| <b>List of Symbols</b>                                    | <b>xiii</b> |
| <br>  |             |
| <b>1 Introduction</b>                                     | <b>1</b>    |
| 1.1 Formation Flying Missions . . . . .                   | 2           |
| 1.2 Motivation, research question and objective . . . . . | 4           |
| 1.3 Thesis Overview . . . . .                             | 6           |
| <br>  |             |
| <b>2 Formation Design</b>                                 | <b>7</b>    |
| 2.1 Non-linear relative motion . . . . .                  | 7           |
| 2.2 Linear relative motion . . . . .                      | 9           |
| 2.3 Relative orbital elements . . . . .                   | 11          |
| <br>  |             |
| <b>3 Software</b>   | <b>17</b>   |
| 3.1 GODOT . . . . .                                       | 17          |
| 3.2 PyGMO . . . . .                                       | 21          |
| <br>  |             |
| <b>4 Methodology</b>                                      | <b>25</b>   |
| 4.1 Preliminary cartwheel analysis . . . . .              | 25          |
| 4.1.1 Formation analysis . . . . .                        | 28          |

|          |                                    |           |
|----------|------------------------------------|-----------|
| 4.1.2    | Transfer analysis . . . . .        | 32        |
| 4.2      | Science phase . . . . .            | 35        |
| 4.3      | Transfer phase . . . . .           | 37        |
| 4.3.1    | First Transfer Strategy . . . . .  | 38        |
| 4.3.2    | Second Transfer Strategy . . . . . | 41        |
| <b>5</b> | <b>Results</b>                     | <b>45</b> |
| 5.1      | Science Phase . . . . .            | 45        |
| 5.2      | Transfer Phase . . . . .           | 52        |
| 5.2.1    | First Transfer Strategy . . . . .  | 52        |
| 5.2.2    | Second Transfer Strategy . . . . . | 54        |
| <b>6</b> | <b>Conclusions</b>                 | <b>59</b> |
|          | <b>Bibliography</b>                | <b>61</b> |

# List of Figures

|      |   |    |
|------|---|----|
| 1.1  | PROBA-3 configuration (image credit: PROBA-3 consortium). . . . .   | 3  |
| 1.2  | Cartwheel formation flying. . . . .   | 5  |
| 2.1  | Rotating Euler-Hill frame. . . . .  | 8  |
| 2.2  | Major characteristic of the cartwheel formation. . . . .  | 13 |
| 2.3  | The outcome motion depending on the selection of $\omega$ . . . . .   | 14 |
| 4.1  | Solar System configuration for the acceleration analysis (not in scale). . . . .                                    | 26 |
| 4.2  | Acceleration analysis considering gravitational, SRP and $J_2$ perturbations. . . . .                               | 27 |
| 4.3  | Difference between True, Osculating and Mean Earth. . . . .   | 28 |
| 4.4  | Geometry evolution in Keplerian model. . . . .  | 29 |
| 4.5  | Geometry evolution in N-body model. . . . .   | 30 |
| 4.6  | Geometry parameters in function of the initial displacement angle. . . . .  | 31 |
| 4.7  | Geometry parameters in function of arm length. . . . .  | 32 |
| 4.8  | Orbital elements evolution. . . . .   | 33 |
| 4.9  | Pork-chop opportunity maps for each satellite. . . . .  | 34 |
| 4.10 | Diagram showing the steps followed to optimize the scientific phase. . . . .  | 37 |
| 4.11 | Condition at infinite defined by $v_\infty$ , $\alpha_\infty$ and $\delta_\infty$ . . . . .                         | 38 |
| 4.12 | Schemes of the optimization problem for the first strategy. . . . .   | 40 |
| 4.13 | Diagram of the optimization process used for the first strategy. . . . .  | 41 |
| 4.14 | Resulting trajectories for the first optimal transfer strategy. . . . .   | 42 |
| 4.15 | Resulting trajectories for the second optimal transfer strategy. . . . .  | 43 |
| 4.16 | Diagram of the optimization process used for the second strategy. . . . .   | 44 |
| 5.1  | Formation with $\theta_0 = -20^\circ$ and $L = 2.5 \times 10^6$ km. . . . .   | 46 |
| 5.2  | Formation with $\theta_0 = 15^\circ$ and $L = 2.5 \times 10^6$ km. . . . .  | 47 |
| 5.3  | Formation with $\theta_0 = -25^\circ$ and $L = 2.5 \times 10^6$ km. . . . .   | 48 |
| 5.4  | Maximum variation comparison between optimized and non-optimized solutions with respect to $\theta_0$ . . . . .     | 50 |
| 5.5  | Maximum variation comparison between $J_{\text{Length}}$ and $J_{\text{Rate}}$ with respect to $\theta_0$ . . . . . | 51 |
| 5.6  | Maximum variation comparison between $J_{\text{Length}}$ and $J_{\text{Rate}}$ with respect to $L$ . . . . .        | 51 |

|      |   |    |
|------|---|----|
| 5.7  | Transfer and science trajectories using the first strategy. . . . .         | 54 |
| 5.8  | Transfer and science trajectories using the second strategy. . . . .        | 55 |
| 5.9  | Geometry evolution during the transfer and part of the science phase. . . . | 56 |
| 5.10 | $\Delta V$ trend for an entire year. . . . .                                | 57 |
| 5.11 | Time of flight variation over a one-year window. . . . .                    | 57 |

## List of Tables

|     |  |    |
|-----|--|----|
| 2.1 | Summary of orbital elements necessary to design the formation. . . . .                     | 15 |
| 4.1 | Min and max deviation of $L$ , $\dot{L}$ and $\alpha$ in Keplerian and N-body model. . . . | 30 |
| 4.2 | Cost and period of the transfer for different $\theta_0$ . . . . .                         | 34 |
| 5.1 | Requirements on the geometry of the formation. . . . .                                     | 45 |
| 5.2 | Results obtained solving Problem 1.1. . . . .  | 53 |
| 5.3 | Results obtained solving Problem 1.2. . . . .  | 53 |
| 5.4 | Results obtained solving Problem 2. . . . .  | 54 |
| 5.5 | Optimization results of July and November. . . . .   | 57 |



# Acronyms

**ARM** Apogee Raising Manoeuvre.

**AU** Astronomical Unit.

**CCSDS** Consultative Committee for Space Data Systems.

**CW** Clohessey–Wiltshire.

**DFACS** Drag Free Attitude Control System.

**DSM** Deep Space Manoeuvre.

**EDHO** Earth Displaced Heliocentric Orbit.

**ELHO** Earth Leading Heliocentric Orbit.

**ETHO** Earth Trailing Heliocentric Orbit.

**FF** Formation Flying.

**GCO** General Circular Orbit.

**GNC** Guidance Navigation and Control.

**GPS** Global Positioning System.

**HGA** High Gain Antenna.

**LGA** Lunar Gravity Assist.

**LISA** Laser Interferometer Space Antenna.

**LVLH** Local-Vertical-Local-Horizontal.

**OEM** Orbit Ephemeris Message.

**RHS** Righth Hand Side.

**ROE** Relative Orbital Elements.

**SAA** Sun Aspect Angle.

**SEP** Solar Electric Propulsion.

**SOI** Sphere Of Influence.

**SRP** Solar Radiation Pressure.

**UDP** User Defined Problem.

## List of Symbols

| Variable        | Description                           | SI unit |
|-----------------|---------------------------------------|---------|
| $a$             | semi major axis                       | km      |
| $e$             | eccentricity                          | -       |
| $i$             | inclination                           | °       |
| $\Omega$        | right-ascension of the ascending node | °       |
| $\omega$        | argument of perigee                   | °       |
| $\theta$        | true anomaly                          | °       |
| $\theta_0$      | initial displacement angle            | °       |
| $\Delta V$      | magnitude of impulsive velocity       | km/s    |
| $v_\infty$      | infinite velocity                     | km/s    |
| $\alpha_\infty$ | infinite right ascension              | °       |
| $\delta_\infty$ | infinite declination                  | °       |
| $r_{SOI}$       | sphere of influence radius            | km      |
| $\gamma$        | vernal equinox                        | -       |



# 1 | Introduction

The space industry contains in itself a fundamental dichotomy between the necessity of making groundbreaking technological and scientific discoveries and the demand of limiting the costs to the essentials. This phenomenon increased when private companies gradually began to invest in the space sector, trying to develop more financially stable models. In the last decades, the launch of formation flying missions increased significantly, trying to reconcile low-budget solutions with innovative results.

Formation flying (FF) can be defined as a multi-satellite mission in which a desired relative attitude and position between the spacecraft is maintained stable or actively controlled. Several benefits can be obtained by using this type of mission, which are here briefly explained. The main advantage is the possibility of dividing the functions of a single spacecraft between the elements composing the formation, adding redundancy to the system. In this sense, the failure of a component or even the loss of one satellite would not jeopardise the formation's performance, while in the case of single spacecraft missions this could result in an early end of operation or the need for manned on-orbit maintenance. Manufacturing multiple smaller satellites, usually very similar or even identical to each other, can simplify and reduce the cost of the production and testing phase compared to a monolithic system [1]. The second reason consists in the high technological and scientific returns of these missions; by assuming specific configurations the formation can achieve high-precision results that could not be obtained otherwise, in particular improving resolution and coverage of Earth-observing missions. In addition, the development of *precision* formation flying is fundamental for the refinement of autonomous rendezvous and docking, on-orbit assembly and servicing. Finally, formation flying not only improves the quality of already achievable results but also gives the possibility of designing configurations capable of measuring and detecting phenomena that with a single satellite could not be observed. In general FF has a set of unique characteristics that can be summarized in these four points [2]:

**Formation Design:** The science objective of the mission dictates a geometry that must be kept during the entire lifetime of the spacecraft. The final goal is to keep the formation as long as possible with no or low fuel consumption.

**Relative Navigation:** Since FF is such only if satellites maintain a relative distance between each other, is necessary to assess the relative positions between two or more members of the fleet to verify that the requirements are all satisfied.

**Inter-satellite Communication:** An exchange of information between the satellites is vital for their survival since the formation control needed to keep the correct distance between the S/C heavily relies on these communications.

**Formation Control:** The formation needs a control system to keep the geometry as intended, especially in highly perturbed orbits.

Generally, formation flying mission can be categorized by the body that is orbited by differentiating between geocentric or heliocentric missions and by the geometry assumed by the fleet during operations; some examples are *trailing*, in which different satellites follow the same trajectory, *tetrahedral*, where four satellites assume a pyramidal configuration and *cartwheel* formation, composed of n-spacecraft orbiting the same relative orbit equally spaced.

## 1.1. Formation Flying Missions

In the last decades, multiple formation flying missions have been launched successfully; in this section, an initial presentation of the most relevant FF missions is followed by a description of the cartwheel formation, a particular type of configuration on which this work is focused on. Two of the earliest missions implementing formation flying technology are ESA's CLUSTER mission and ESA/NASA GRACE mission, launched respectively in 2000 and 2002. The Cluster mission is composed of four identical spacecraft to study small-scale plasma structures at the boundaries of the magnetosphere. The satellites are injected into highly elliptical polar orbits, designed to obtain a tetrahedral configuration, ideal to measure the three-dimensional plasma structures in the different regions of Earth's magnetic field. The necessity of collecting three-dimensional measurements imposes the type of configuration assumed by the satellites since one or two-spacecraft missions are capable of obtaining only one-dimensional measures [3]. After over 20 years of observations, the Cluster mission provided a deeper understanding of the magnetosphere thanks to its unique architecture. Cluster's main achievements consisted of a more complete investigation of the solar wind and the turbulence associated with this phenomenon, observations of the magnetic reconnection process and in-depth analysis of space weather and geomagnetic storms, making it one of the most successful ESA's mission<sup>1</sup>.

---

<sup>1</sup>[https://www.esa.int/Science\\_Exploration/Space\\_Science/Cluster/Cluster\\_s\\_20\\_years\\_of\\_studying\\_Earth\\_s\\_magnetosphere](https://www.esa.int/Science_Exploration/Space_Science/Cluster/Cluster_s_20_years_of_studying_Earth_s_magnetosphere)

DLR and NASA developed the GRACE mission which features two identical satellites, GRACE-1 and GRACE-2, in a leader-follower configuration on circular polar co-planar orbits. The purpose of this mission is to obtain a high-fidelity model of Earth's gravity field by measuring the spatial and temporal alteration of its mass. The mean inter-satellite distance between the two units is 220 km with variations of  $\pm 50$  km; the key mission's instrument, Ka-Band Ranging System, measures this separation which is a direct expression of the gravitational variations due to a non-homogeneous mass distribution [4]. GRACE mission provided fundamental insights into the relationship between oceans and land in terms of mass redistribution around the globe. The constant mapping of the gravity variations offered helpful information on the loss of ice mass in the polar regions, the sea level rise, underground water sources and solid Earth changes<sup>2</sup>.

Formation Flying missions are not only widely used for investigating scientific goals but can be also employed as technological demonstrators like PROBA-3 and PRISMA, both developed under ESA's supervision. PROBA-3 is a technological demonstrator for precise formation flying, consisting of two small spacecraft keeping a distance between 25 to 250 meters and controlling the relative position with accuracy in the order of one millimetre. Such configuration, if successful, could set the path for a new multi-satellite mission in which the fleet acts as a single structure, with the possibility of improving different fields such as Earth-observation, in-orbit servicing, deorbiting and automated rendezvous and docking [5].

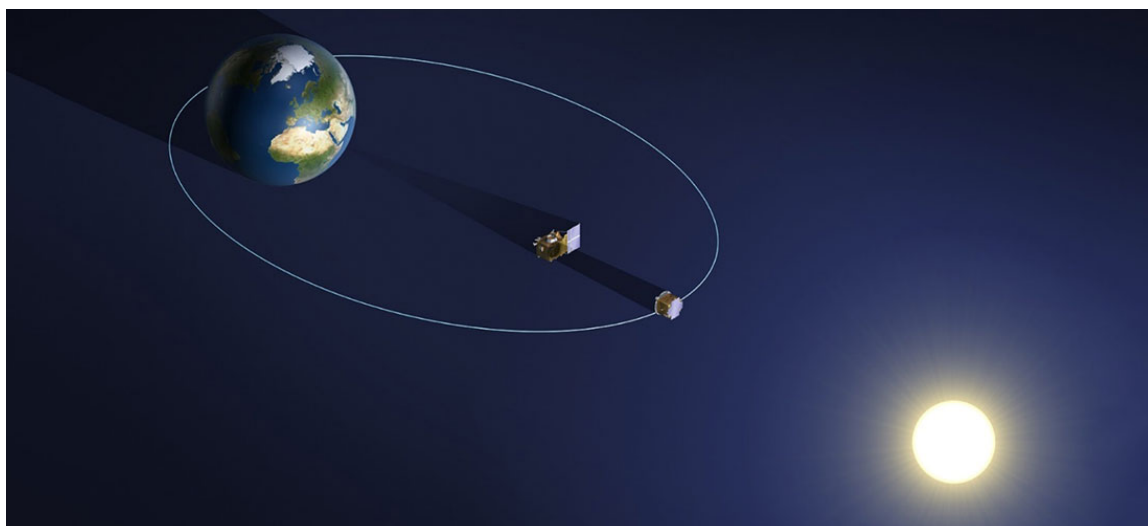


Figure 1.1: PROBA-3 configuration (image credit: PROBA-3 consortium).

---

<sup>2</sup><https://www.jpl.nasa.gov/news/prolific-earth-gravity-satellites-end-science-mission>

PRISMA mission's objective is to test Guidance, Navigation and Control (GNC) capabilities for formation flying and rendezvous. The mission consists of two satellites, one called MAIN with high manoeuvrability and one called TARGET with no orbit manoeuvring capability; once in orbit, for 8–10 months, a continuous sequence of experiments ranging from autonomous formation flying using GPS to rendezvous and proximity operations using vision-based systems. This mission manages to test and validate different algorithms, sensors and actuators in the formation flying framework [6, 7].

## Cartwheel formation

Formation flying missions are not limited to geocentric orbits, but can be applied to different kinds of orbits such as heliocentric ones; the most remarkable example is Laser Interferometer Space Antenna (LISA), programmed to be launched in 2034. LISA is the third L class mission selected in the ESA Cosmic Vision 2015-2025 plan with the objective of detecting and measuring gravitational waves with frequencies between 0.1 mHz and 1 Hz, undetectable on Earth due to limitation of the instruments' length and gravity gradient noise. The formation assumed for this mission, as shown in Fig. 1.2, is called cartwheel formation flying, which in general can be described as  $n$  satellites on individual orbits uniformly distributed on an ellipse centred on the formation centre. In the case of LISA, three identical satellites orbit the Sun in a trailing Earth Displaced Heliocentric Orbit (EDHO) with a distance from Earth between 50 and 65 million km and an inter-satellite distance of 2.5 million km. The objective of the mission design is to maintain the formation within the limit imposed by the mission requirements on arm length  $L$  (relative distance between the satellites), arm length rate  $\dot{L}$  (relative velocity between the satellites) and corner angle  $\alpha$  (angle between the arms of the formation). What makes this mission unique is that the spacecraft need to follow the two test masses contained in each S/C which are subjected only to gravitational acceleration; all non-gravitational accelerations, including Solar Radiation Pressure, are counteracted by the Drag-Free Attitude Control System (DFACS), meaning that only gravitational acceleration affects the motion of the spacecraft [8, 9].

## 1.2. Motivation, research question and objective

LISA is a unique mission due to its payload, the dynamic conditions under which operates and its high-level requirements needed to gather successfully all the data, meaning that a more general understanding of the cartwheel configuration is needed in case other missions target similar formation with different scientific requirements and payloads. Mis-

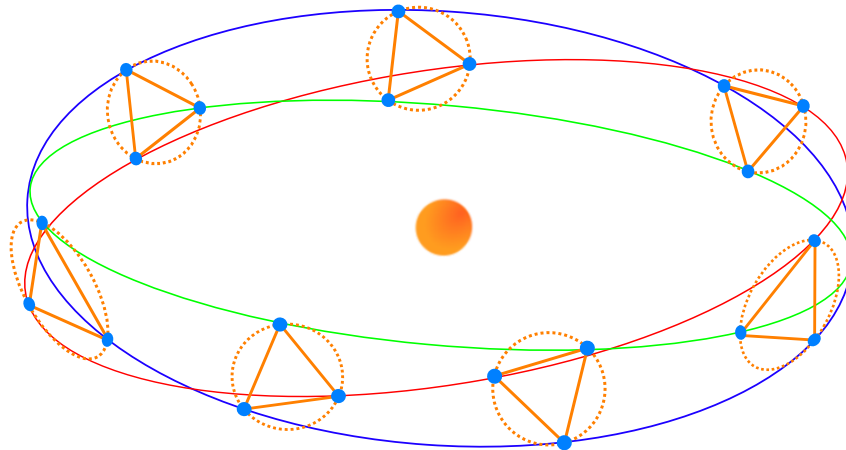


Figure 1.2: Cartwheel formation flying.

sions taking advantage of this cartwheel configuration are currently being proposed, with ALBATROS being the most remarkable example. The objective of this mission consists of an all-sky monitoring of high-energy events with particular attention on obtaining a substantial sample of Gamma Ray Bursts [10]. The focus of this work is centred on defining different optimization strategies both for the formation design and the transfer of the fleet. In particular, to generalize the problem with respect to LISA, a complete dynamic including non-gravitational forces is considered both for the optimization of the formation and the transfer. This work has been developed to answer the following question:

How can we design a cart-wheel formation maximizing its stability  
and achieve the best strategies to transfer it?

The first layer of complexity of this problem is given by the fact that three individual satellites must be optimized both for the formation design and the transfer. The units of the fleet composing the cartwheel formation belong to the SmallSat class, meaning that the mass ranges from 100 kg to 500 kg; with this mass all spacecraft can be launched using a single launcher, implying that is necessary to find a way to reconcile the initial transfer phase in which the satellites are all stowed in the launch vehicle with a null inter-satellite distance, with the scientific phase in which the nominal arm length for a LISA-like mission is 2.5 million km. The equilibrium between the two phases is of high priority to assure a stable formation and a low-cost transfer. For this reason to avoid dealing with a single optimization problem taking care of both phases simultaneously the problem is split into two simpler objectives ensuring a lower level of complexity. The three main focus points are a preliminary analysis of formation stability and transfer costs, the definition of an optimization procedure to stabilize the formation and the selection of a transfer strategy.

These objectives are:

1. Preliminary analysis on formation design and transfer: the parameters affecting the evolution of the geometry characteristics of the fleet are studied to better understand the behaviour of the cartwheel formation. In addition, an initial analysis of the transfer is needed to gain general knowledge on the main figure of merit of the transfer, such as  $\Delta V$  and time of flight.
2. Develop an optimization routine to maintain the formation stable. The geometry and its variation are defined by the science objectives which can vary from mission to mission; the performances of the optimization are measured in terms of variation of arm length, arm length rate and corner angle with respect to the nominal values.
3. Develop an optimal transfer strategy to deploy the three S/C in their final orbits. The complexity of such problem relies mainly on the fact that each satellite is independent from the others from a certain epoch onward, increasing the degrees of freedom of the problem.

### 1.3. Thesis Overview

The thesis is structured as follows. In Chapter 2 the theoretical background for formation flying is presented starting from the equations of relative motion necessary to describe FF. In Chapter 3 the environment in which the work is developed, GODOT and PyGMO, is described and the most important and used features are discussed with more attention. In Chapter 4 a first general presentation of the problem is followed by a more detailed analysis of the approaches used to optimize the formation maintenance and transfer. In Chapter 5 the results of the optimizations are presented and finally, in Chapter 6, the conclusions and possible future development are stated.

# 2 | Formation Design

This chapter collects the main theoretical topics which support this work. A review of state-of-the-art formation flying concepts is presented, in which different models of relative motions are presented and analysed to achieve a mathematical description of the cartwheel formation. The objective of this chapter is to retrieve the relations between orbital elements in such a way that the cartwheel formation is fully described; starting from non-linear relative motion, the equations are linearized and then parameterized with respect to relative orbital elements (ROE) through which a description of the formation can be obtained.

## 2.1. Non-linear relative motion

The first step to define the cartwheel configuration is to find the equations that characterize the relative motion of a satellite. Let's consider two spacecraft orbiting the same body and refer to them as chief and deputy. This nomenclature is used to describe a general motion between two satellites with respect to the more specific leader/follower and target/chaser, respectively used for in-line formation flying and orbital rendezvous. The objective is to describe the motion of the deputy with respect to the chief, which can be a real satellite or a fictitious point in space like in the cartwheel formation. The relative motion equations are defined using Keplerian two-body dynamic, first in the inertial frame and then in the Euler-Hill frame. The inertial frame is centred at the primary and the axis are defined as follows:  $\hat{x}$  is directed from the main body's centre along the vernal equinox,  $\hat{z}$  is normal to the plane, positive in the north direction and  $\hat{y}$  complete the coordinate system. The Euler-Hill frame is instead an LVLH rotating system with the origin on the chief satellite, in which the  $\hat{x}$  component is directed from the spacecraft radially outward, the  $\hat{z}$  component is normal to the orbital plane and the  $\hat{y}$  component complete the right-handed coordinate system as shown in Fig. 2.1; this frame will be referred to as  $\mathcal{L}$ . Note that in the equations any quantity associated with the chief will be indicated using  $(\cdot)_0$ , while for the deputy  $(\cdot)_1$  will be used.

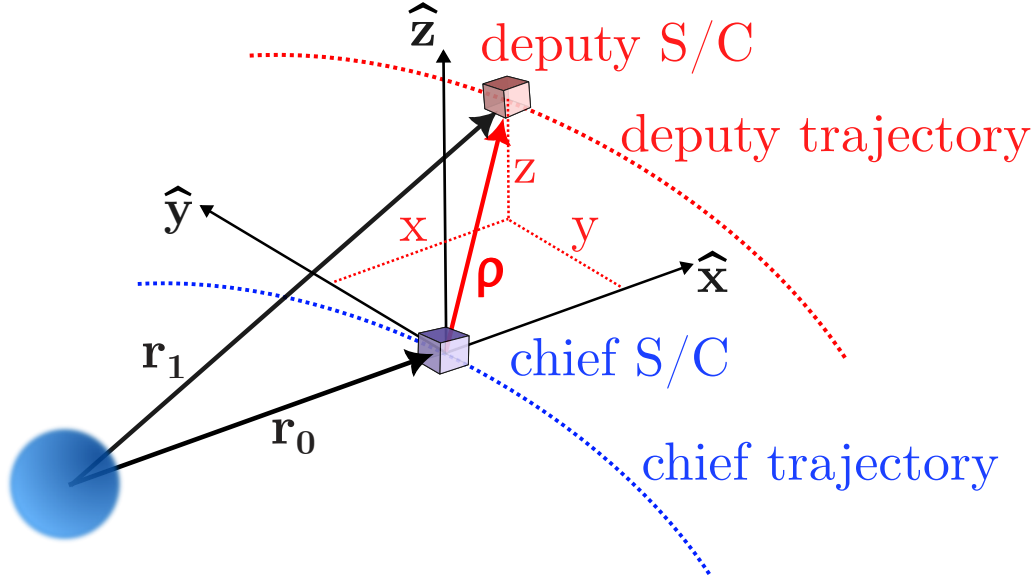


Figure 2.1: Rotating Euler-Hill frame.

The inertial equations that describe the motion of the chief and deputy are

$$\begin{aligned}\ddot{\mathbf{r}}_0 &= -\frac{\mu}{r_0^3}\mathbf{r}_0 & \text{where } r_0 &= \|\mathbf{r}_0\| \\ \ddot{\mathbf{r}}_1 &= -\frac{\mu}{r_0^3}\mathbf{r}_1 & \text{where } r_1 &= \|\mathbf{r}_1\|\end{aligned}$$

while, given that the relative position of the deputy with respect to the chief is  $\boldsymbol{\rho} = \mathbf{r}_1 - \mathbf{r}_0$ , then the relative acceleration is

$$\ddot{\boldsymbol{\rho}} = -\frac{\mu(\mathbf{r}_0 + \boldsymbol{\rho})}{\|\mathbf{r}_0 + \boldsymbol{\rho}\|^3} + \frac{\mu}{r_0}\mathbf{r}_0$$

To define the relative acceleration between the two frames we can recall that

$$\ddot{\boldsymbol{\rho}} = \ddot{\boldsymbol{\rho}}_{\mathcal{L}} + 2\boldsymbol{\omega}_{\mathcal{L}} \times \dot{\boldsymbol{\rho}}_{\mathcal{L}} + \dot{\boldsymbol{\omega}}_{\mathcal{L}} \times \boldsymbol{\rho} + \boldsymbol{\omega}_{\mathcal{L}} \times (\boldsymbol{\omega}_{\mathcal{L}} \times \boldsymbol{\rho}) \quad (2.1)$$

where  $\boldsymbol{\omega}_{\mathcal{L}}$  is the angular velocity vector of the Euler-Hill frame relative to the inertial one. The component-wise equations for the relative motions can be obtained substituting

$$\begin{aligned}\boldsymbol{\omega}_{\mathcal{L}} &= [0, 0, \dot{\theta}_0]^T \\ \mathbf{r}_0 &= [r_0, 0, 0]^T\end{aligned}$$

in Eq. 2.1, yielding to the following

$$\begin{aligned}
\ddot{x} - 2\dot{\theta}_0\dot{y} - \ddot{\theta}_0y - \dot{\theta}_0^2x &= -\frac{\mu(r_0 + x)}{[(r_0 + x)^2 + y^2 + z^2]^{\frac{3}{2}}} + \frac{\mu}{r_0^2} \\
\ddot{y} + 2\dot{\theta}_0\dot{x} + \ddot{\theta}_0x - \dot{\theta}_0^2y &= -\frac{\mu y}{[(r_0 + x)^2 + y^2 + z^2]^{\frac{3}{2}}} \\
\ddot{z} &= -\frac{\mu z}{[(r_0 + x)^2 + y^2 + z^2]^{\frac{3}{2}}}
\end{aligned} \tag{2.2}$$

where  $\boldsymbol{\rho}_{\mathcal{L}} = [x, y, z]^T$ .

## 2.2. Linear relative motion

Eqs. 2.2 can be simplified by assuming that the chief is on a circular orbit around the primary, which is usually an acceptable assumption. In this case  $\dot{\theta}_0 = n_0 = \sqrt{\frac{\mu}{a_0^3}}$ ,  $\ddot{\theta}_0 = 0$  and  $r_0 = a_0 = \text{const}$ , that substituted in Eqs. 2.2, yields to:

$$\begin{aligned}
\ddot{x} - 2n_0\dot{y} - n_0^2x &= -\frac{\mu(a_0 + x)}{[(a_0 + x)^2 + y^2 + z^2]^{\frac{3}{2}}} + \frac{\mu}{a_0^2} \\
\ddot{y} + 2n_0\dot{x} - n_0^2y &= -\frac{\mu y}{[(a_0 + x)^2 + y^2 + z^2]^{\frac{3}{2}}} \\
\ddot{z} &= -\frac{\mu z}{[(a_0 + x)^2 + y^2 + z^2]^{\frac{3}{2}}}
\end{aligned} \tag{2.3}$$

which is a system of non-linear equations describing the motion of the deputy relative to the chief satellite orbiting on a circular trajectory [11]. These equations can be further simplified by linearizing them with respect to the circular orbit, obtaining the so called Clohessey–Wiltshire (CW) equations. By expanding the right-hand side (RHS) of Eqs. 2.3 and linearizing about the origin of the chief-fixed frame the following results are obtained

$$\begin{aligned}
-\frac{\mu(a_0 + x)}{[(a_0 + x)^2 + y^2 + z^2]^{\frac{3}{2}}} &\approx n_0^2(2x - a_0) \\
-\frac{\mu y}{[(a_0 + x)^2 + y^2 + z^2]^{\frac{3}{2}}} &\approx -n_0^2y \\
-\frac{\mu z}{[(a_0 + x)^2 + y^2 + z^2]^{\frac{3}{2}}} &\approx -n_0^2z
\end{aligned}$$

Then, the CW equations then can be written as

$$\begin{aligned} \ddot{x} - 2n_0\dot{y} - 3n_0^2x &= 0 \\ \ddot{y} + 2n_0\dot{x} &= 0 \\ \ddot{z} + n_0^2z &= 0 \end{aligned} \quad (2.4)$$

The closed-form solution of these equations, where  $c_{nt} = \cos(nt)$ ,  $s_{nt} = \sin(nt)$  and the subscript 0 is removed, meaning  $n_0 = n$ , is given by:

$$\begin{pmatrix} x(t) \\ y(t) \\ z(t) \\ \dot{x}(t) \\ \dot{y}(t) \\ \dot{z}(t) \end{pmatrix} = \begin{bmatrix} 4 - 3c_{nt} & 0 & 0 & \frac{1}{n}s_{nt} & \frac{2}{n}(1 - c_{nt}) & 0 \\ 6(s_{nt} - nt) & 1 & 0 & -\frac{2}{n}(1 - c_{nt}) & \frac{1}{n}(4s_{nt} - 3nt) & 0 \\ 0 & 0 & c_{nt} & 0 & 0 & \frac{1}{n}s_{nt} \\ 3ns_{nt} & 0 & 0 & c_{nt} & 2s_{nt} & 0 \\ -6n(1 - c_{nt}) & 0 & 0 & -2s_{nt} & 4c_{nt} - 3 & 0 \\ 0 & 0 & -ns_{nt} & 0 & 0 & c_{nt} \end{bmatrix} \begin{pmatrix} x_0 \\ y_0 \\ z_0 \\ \dot{x}_0 \\ \dot{y}_0 \\ \dot{z}_0 \end{pmatrix} \quad (2.5)$$

Some critical observations can be made. From Eqs. 2.4 it is clear that the motion along the  $\hat{z}$  direction, also referred to as ‘out-of-plane’ or ‘cross-track’ motion is decoupled from the one in the  $\hat{x}$ - $\hat{y}$  direction. As can be seen in the solution in Eq. 2.5 the cross-track motion is a harmonic motion that can be cancelled by considering as initial conditions  $z(0) = \dot{z}(0) = 0$ .

The along-track motion shows a drift which varies linearly with time, meaning that the motion in the  $\hat{y}$  direction is unstable. It is possible to find a stable sub-space for which this drift is nullified, obtained with the following initial condition:  $\dot{y}_0 = -2nx_0$ . This assumption is needed since the objective is to obtain the motion of the deputy bounded, even if only in first approximation, to the one of the chief.

The characteristics of a formation are usually defined by some geometric constraints, meaning that these equations need further analysis to obtain geometric insight. To do so Eqs. 2.4 can be rewritten in magnitude/phase form as

$$\begin{aligned} x(t) &= \rho_x \sin(nt + \alpha_x) \\ y(t) &= \rho_y + 2\rho_x \cos(nt + \alpha_x) \\ z(t) &= \rho_z \sin(nt + \alpha_z) \end{aligned} \quad (2.6)$$

where

$$\begin{aligned}
\rho_x &= \frac{\sqrt{(\dot{x}^2(0) + x^2(0))n^2}}{n} \\
\rho_y &= y(0) - \frac{2\dot{x}(0)}{n} \\
\rho_z &= \frac{\sqrt{(\dot{z}^2(0) + z^2(0))n^2}}{n} \\
\alpha_x &= \arctan \frac{nx(0)}{\dot{x}(0)} \\
\alpha_z &= \arctan \frac{nz(0)}{\dot{z}(0)}
\end{aligned} \tag{2.7}$$

Through this formulation, by setting up relations between the parameters defined in Eqs. 2.7, is possible to geometrically characterize the relative motion [12]. In general the in-plane motion in the  $\hat{x} - \hat{y}$  plane is a ellipse with semi-major axis  $2\rho_x$ , semi-minor axis  $\rho_x$  and constant eccentricity  $\sqrt{1 - \rho_x^2/(4\rho_x^2)} = \sqrt{3}/2$ . A more interesting result is obtained by choosing  $\alpha_x = \alpha_z$  and  $\rho_z = \pm\sqrt{3}\rho_x$ , which leadsto a relative circular orbit with radius  $2\rho_x$ , called general circular orbit (GCO) [13]. These circular orbits are inclined by  $60^\circ$  with respect to the orbital plane of the chief satellite and can be used to construct the cartwheel formation. Recalling that the formation under study is composed of three spacecraft forming an equilateral triangle, is possible to design the fleet by distributing on a circular orbit relative to a fictitious centre the three satellites with a phase between each other of  $120^\circ$ .

### 2.3. Relative orbital elements

The last step consists in moving the description of the relative motion from Cartesian coordinates to a set of ROE defined as follows:

$$\delta\alpha = \begin{pmatrix} \delta a \\ \delta\lambda \\ \delta e_x \\ \delta e_y \\ \delta i_x \\ \delta i_y \end{pmatrix} = \begin{pmatrix} (a^{(j)} - a_0)/a_0 \\ (u^{(j)} - u_0) + (\Omega^{(j)} - \Omega_0) \cos i_0 \\ e_x^{(j)} - e_{x0} \\ e_y^{(j)} - e_{y0} \\ i^{(j)} - i_0 \\ (\Omega^{(j)} - \Omega_0) \sin i_0 \end{pmatrix} \tag{2.8}$$

where the subscript 0 refers to the chief orbit and the superscript j to a generic spacecraft of the formation. The vector of relative orbital elements is composed of:  $\delta a$ , the normalized semi-major axis difference,  $\delta\lambda$ , the relative mean longitude defined using the

mean argument of latitude  $u = \omega + M$ , while the remaining quantities are respectively the components of the eccentricity and inclination vectors which in polar notation are

$$\delta \mathbf{e} = \begin{pmatrix} \delta e_x \\ \delta e_y \end{pmatrix} = \delta e \begin{pmatrix} \cos \phi \\ \sin \phi \end{pmatrix} \quad \delta \mathbf{i} = \begin{pmatrix} \delta i_x \\ \delta i_y \end{pmatrix} = \delta i \begin{pmatrix} \cos \psi \\ \sin \psi \end{pmatrix} \quad (2.9)$$

where  $\phi$  and  $\psi$  are referred to as relative perigee and relative ascending node. The objective is to parameterize the CW equations using the relative orbital elements; it is possible to demonstrate a correspondence between the integration constants in Eqs. 2.7 and the relative orbital elements defined in Eq. 2.8, under the assumption of near-circular orbit of the chief spacecraft and small relative radius compared to the one of the chief in the inertial frame<sup>1</sup> [14]. It is important to note that the relative orbital elements defined in Eqs. 2.8 are dimensionless, while the integration constants of the CW equations for rectilinear coordinates have the dimension of a length, meaning that the correlation between the two exists when the quantities are normalized with respect to the semi-major axis of the chief orbit. The relative motion for near-circular orbits using relative orbital elements can be described in general as

$$\begin{aligned} \frac{x}{a} &\approx \delta a - \delta e \cos(u - \phi) \\ \frac{y}{a} &\approx -\frac{3}{2}\delta a(u - u_0) + \delta \lambda + 2\delta e \sin(u - \phi) \\ \frac{z}{a} &\approx \delta i \sin(u - \psi) \end{aligned} \quad (2.10)$$

By adding the bounded motion condition, which, for relative orbital elements, consists in  $\delta a = 0$  and  $\Delta u = -\Delta \Omega \cos i$ , equivalent to  $\delta \lambda = 0$ , the deputy follows an elliptic trajectory around the chief with semi-major axis  $2a \delta e$  in along-track direction and semi-minor axis  $a \delta e$  in radial direction [15].

Now it is possible to build up the conditions on the orbital elements that define the cart-wheel formation. The first step is to recall that the fleet is on an EDHO meaning that the centre of the formation is displaced by a given angle, referred to as  $\theta_0$ , with respect to the Earth's position. This angle in this work is defined as the difference between the initial mean heliocentric longitude of the formation centre with respect to the mean Earth and can assume both positive and negative values generating respectively leading and trailing configurations. The heliocentric mean longitude can be defined as  $l_0 = u_0 + \Omega_0 = \omega_0 + M_0 + \Omega_0$ , while as said the  $\theta_0 = l_0 - l_{ME}$  [16]. The definition of

---

<sup>1</sup>Note that there are only five integration constants coming from the Cartesian CW equations and six relative orbital elements; this is due to the fact that the CW equations shown in 2.6 are already simplified to describe a bounded relative motion.

the displacement angle used in this thesis diverges slightly from the one of other works in which this angle is referred to as Mean Instantaneous Displacement Angle, defined by taking as a reference the mean Earth-Moon barycentre, instead of the mean Earth. This difference will not cause any major mismatch since, as presented in Section 4.2, the initial orbital elements are used only as initial guess for the optimization.

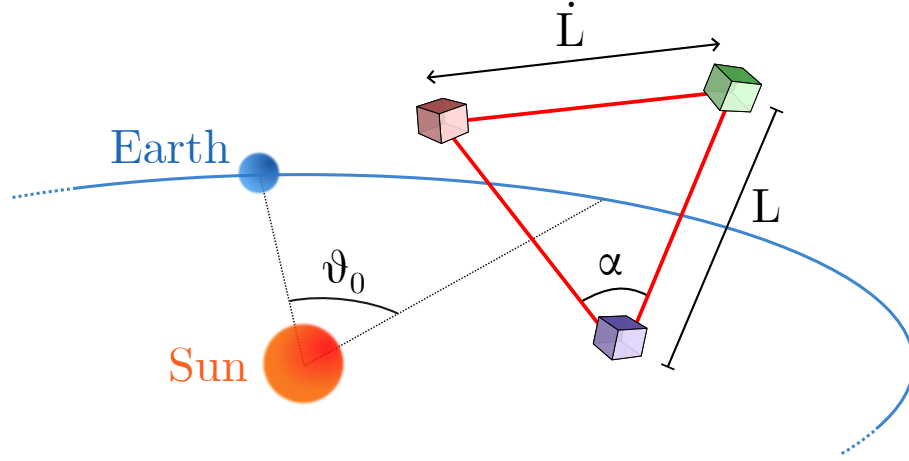


Figure 2.2: Major characteristic of the cartwheel formation.

The chief of this formation is a fictitious point in the geometric centre of the triangle formed by the fleet, which follows a circular heliocentric orbit with a distance of 1 AU from the Sun, meaning that

$$a_0 = 1 \text{ AU}$$

$$e_0 = 0$$

$$i_0 = 0^\circ$$

Imposing the bounded motion condition,  $\delta a = 0$ , leads to  $a^{(j)} = a_0 = 1 \text{ AU}$ , while with the relation between  $\rho_x$  and  $\rho_z$  an the nominal arm length is possible to define the relative inclination and eccentricity as

$$\begin{aligned} \delta i^{(j)} &= \sqrt{3} \delta e^{(j)} \\ \delta e^{(j)} = e^{(j)} &= \frac{L}{2a_0\sqrt{3}} \end{aligned}$$

Now it is possible to add the other condition which grants the formation of a GCO,  $\alpha_x = \alpha_z$ , equivalent to having a perpendicularity condition between relative eccentricity and inclination vector,  $\phi = \psi + \frac{k\pi}{2}$ ,  $k \in 2\mathbb{Z} + 1$ . From this equation is possible to identify

the other relative orbital elements using the definition in Eq. 2.8:

$$\begin{aligned} \text{From } i_0 = 0 &\implies \sin i_0 = 0 \\ &\implies \delta i_y = \delta i^{(j)} \sin \psi = 0 \\ &\implies \psi = n\pi, n \in \mathbb{Z} \end{aligned}$$

Recalling that the eccentricity vector is defined as

$$\mathbf{e} = \begin{pmatrix} e_x \\ e_y \end{pmatrix} = e \begin{pmatrix} \cos \omega \\ \sin \omega \end{pmatrix}$$

and using the perpendicularity condition between  $\delta \mathbf{e}$  and  $\delta \mathbf{i}$ , follows that  $\delta e_x = 0$ , leading to only two values of argument of perihelion that can satisfy this result:  $\omega^{(j)} = \frac{\pi}{2}$  or  $\omega^{(j)} = \frac{3\pi}{2}$ . These values of  $\omega$  define two types of cartwheel formation, which can be explained by looking at the motion of the cartwheel from the Sun: for  $\omega = \frac{3\pi}{2}$  the motion of the three satellites is clockwise, while for  $\omega = \frac{\pi}{2}$  it is counter-clockwise.

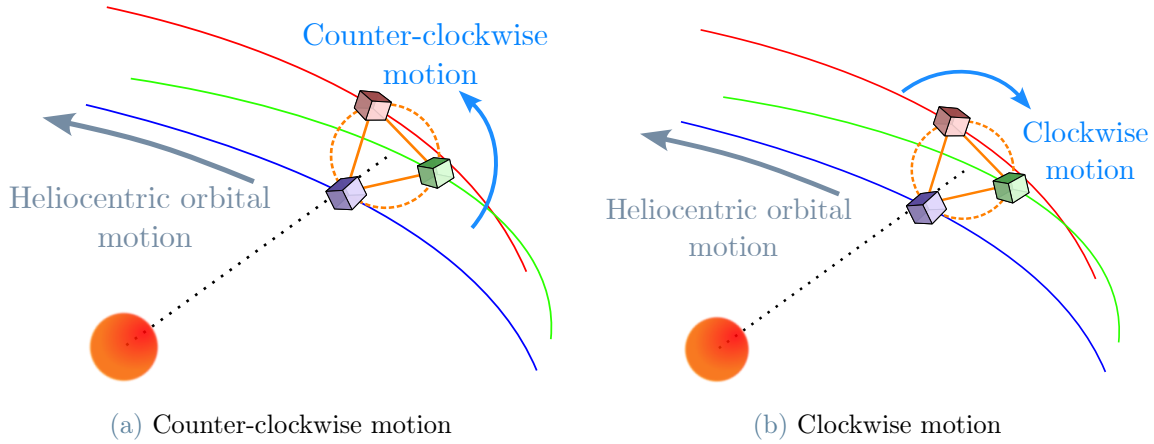


Figure 2.3: The outcome motion depending on the selection of  $\omega$ .

The fleet assumes the desired configuration if all three spacecraft have the same initial mean longitude, which is equal to the one of the formation centre, defined by  $l_0$ . Therefore, there is just one remaining degree of freedom to fully define the fleet's geometry, the RAAN or the mean anomaly of a single satellite, through which is possible to set the phase angle between each element of the formation. With a phase angle equals to  $2\pi/3$  the satellites uniformly distribute on the relative circular orbit around the centre forming an equilateral triangle configuration. In this work the selected free parameter is the RAAN of the first satellite and by changing its values the only variation that occurs to the geometry is a

relative rotation of all satellites around the formation centre. The ecliptic orbital elements of the three spacecraft and the formation centre are reported in Table 2.1.

| SC     | Semi-major axis          | Eccentricity               | Argument of Perihelion               |
|--------|--------------------------|----------------------------|--------------------------------------|
| Centre | $a_0 = 1 \text{ AU}$     | $e_0 = 0$                  | $\omega_0 = 0$                       |
| SC1    | $a^{(1)} = 1 \text{ AU}$ | $e^{(1)} = L/2a_0\sqrt{3}$ | $\omega^{(1)} \in \{\pi/2, 3\pi/2\}$ |
| SC2    | $a^{(2)} = 1 \text{ AU}$ | $e^{(2)} = e^{(1)}$        | $\omega^{(2)} = \omega^{(1)}$        |
| SC3    | $a^{(3)} = 1 \text{ AU}$ | $e^{(3)} = e^{(1)}$        | $\omega^{(3)} = \omega^{(1)}$        |

| SC     | Inclination           | RAAN                                   | Mean anomaly                                  |
|--------|-----------------------|--|---|
| Centre | $i_0 = 0$             | $\Omega_0 = 0$                         | $M_0 = \text{MIDA} + l_{\text{MEMB}}$         |
| SC1    | $i^{(1)} = e\sqrt{3}$ | $\Omega^{(1)} \in \mathbb{R}$          | $M^{(1)} = l_0 - \omega^{(1)} - \Omega^{(1)}$ |
| SC2    | $i^{(2)} = i^{(1)}$   | $\Omega^{(2)} = \Omega^{(1)} - 2\pi/3$ | $M^{(2)} = M^{(1)} + 2\pi/3$                  |
| SC3    | $i^{(3)} = i^{(1)}$   | $\Omega^{(3)} = \Omega^{(1)} - 4\pi/3$ | $M^{(3)} = M^{(1)} + 4\pi/3$                  |

Table 2.1: Summary of orbital elements necessary to design the formation.



# 3 | Software

In this section, the two libraries used to develop the work are briefly presented, discussing and showing the implementation of the main functionalities. On a basic level, to solve the problem outlined in the research question is necessary to perform trajectory propagations and optimizations. GODOT takes care of everything related to the propagation from the epochs definition to the development of the dynamic in which the satellites have to fly, adding the necessary gravitational and non-gravitational accelerations. GODOT is widely used at operational levels at ESOC and can be thought of as a more complete alternative to SPICE. PyGMO deals with the optimization part and provides a simple interface to implement and solve any kind of optimization problem, even if it is tailored to work with aerospace-related problems, making it perfectly suited to this context. In the following sections, more details on these two tools and software are given.

## 3.1. GODOT

GODOT, acronym of General Orbit Determination and Optimization Toolkit, is an application at ESA/ESOC for flight dynamics. The software is coded in C++, but can be used with a Python interface and is still in development; the version on which the code runs on is 0.10.0. This application is formed by three main libraries, each one with specific directories dedicated to a single theme. These three libraries are:

- *Core* contains general directories without a common relation between them (e.g. constant and epoch definition, astrodynamics computations and numerical utilities).
- *Model* defines the frames and points that need to be propagated.
- *Cosmos* is the place where the actual modelling of the dynamic takes place.

GODOT contains a lot of libraries dedicated to all sort of problems, but only the most essential are here reported and briefly discussed.

**Tempo:** this library is fundamental since it handles all time computations involved in GODOT. The main element is the *Epoch* constructor through which time can be defined

using different time scale such as TDB, TAI and UT. The epoch is coded using the following line:

```
t0 = tempo.Epoch('2020-05-14T00:00:00.0000 TDB')
```

**Universe:** This is one of the most important functionalities of GODOT; through this class is possible to set up the environment where all the propagation, estimation and optimization problems are carried out. The *Universe* is defined by a series of plug-ins, each one taking care of a single aspect of the environment that the user wants to develop. The *Universe* object is created through a .json or .yaml file which needs to be validated against a schema available on the GODOT site<sup>1</sup>. Below are reported only the mandatory and most relevant plug-ins:

- Version plug-in: configures the file version.
- Spacetime plug-in: defines the space-time coordinates for the solar system, BCRS (Barycentre Celestial Reference System) for simulations ‘far’ from Earth and GCRD (Geocentric Barycentre Celestial Reference System) for models ‘near’ Earth.
- Ephemeris plug-in: uploads, using kernels, all the ephemerides that are needed for the modelling; constants, frames and bodies are all extracted from this plug-in.
- Frames plug-in: defines axes and points that are not defined by default in GODOT. The only frames and points automatically created are ICRF (Inertial Celestial Reference Frame), EMC (Earth Mean eClyptic frame) and SSB (Solar System Barycentre), other frames can be added using the *Orient* library, while points can be generated using TLEs, Keplerian elements, IPF or OEM files.
- Constants plug-in: collects constants of different nature, mathematical (e.g. Pi, Deg and Rad conversion), physical (e.g. Astronomical Unit, Speed of Light) and body constants (e.g. gravitational constants, radii, and spheres of influence of bodies).
- Bodies plug-in: sets up the bodies that need to be taken into consideration during the gravitational acceleration computation.
- Gravity plug-in: configures the gravity that will influence the spacecraft during numerical propagation; in addition, it is possible to configure a structure of bodies that can automatically take care of switching the center of integration in case the satellite crosses a sphere of influence.
- Dynamics plug-in: adds all the accelerations that the propagator needs to consider (gravitational, solar radiation pressure and drag).

---

<sup>1</sup><https://godot.io.esa.int/docs/0.10.0/index.html>

- Spacecraft plug-in: collects all the characteristics of the spacecraft that need to be propagated, mass, cross-section area, drag and reflectivity coefficient, thruster parameters and many others.

The *Universe* object can be created using the following code:

```
uni_config = cosmos.util.load_yaml('.../path_to_file/Universe.yml')
uni = cosmos.Universe(uni_config)
```

**Trajectory:** It is worth mentioning a powerful method to initialise and propagate elements of a trajectory (such as state, mass and  $\Delta V$ ) using the *Trajectory* class, even if is not used extensively in this work. The setup is similar to the one of the *Universe* and it is computed using .json or .yaml files; the main part of the configuration is the timeline which contains a chronological list of all the trajectory steps. There are different types of timeline, each one with a specific use:

- Control: these points are characterized by a known state, input by the user, from which the propagation can begin, in both directions, forward or backward.
- Point: these allow the introduction of a discontinuity in the state and can be used as an initial or final point for the propagation.
- Manoeuvre: these points are similar to the one just described, but it is possible to introduce an acceleration to the spacecraft.
- Match: in case multiple Control points are given a Match point must be inserted between these and a constraint must be added to assure a continuous trajectory.

The other parts consist of *Setting* which defines the tolerances, the integration method and the maximum steps available to the propagator and *Setup* which setups the quantities that need to be integrated. Similarly to the *Universe*, the *Trajectory* object is created as follow:

```
tra_config = cosmos.util.load_yaml('.../path_to_file/Trajectory.yml')
tra = cosmos.Trajectory(uni, tra_config)
```

**Propagator:** GODOT offers two alternatives to propagate quantities respect to the *Trajectory* class, which do not require any external file: *BallisticPropagator* and *Propagator*. Here the attention moves to the other methods which are used more extensively in the development of this work.

*BallisticPropagator* is a tool defined in the *Cosmos* library and allows the propagation of position and velocity (not mass and  $\Delta V$ ) of a spacecraft with the dynamic defined in the plug-ins of the *Universe*. To implement this kind of propagator and extract the state

information the necessary code is the following:

```
pro = cosmos.BallisticPropagator(uni, 'SC', 'Dynamic', t0, 'Body', tol)
pro.compute(x0, dt0, tf)
x = uni.frames.vector6('wrt_Body', 'SC', 'Frame', tf)
```

where the variable `uni` is the *Universe* object, `'SC'` and `'Dynamic'` are the names of the satellite and dynamic defined in the *Spacecraft* and *Dynamic* plug-ins of the *Universe*, `t0` and `tf` are respectively the initial and final epoch, `'Body'` is the name of the body to which the in initial state is given (the center of integration), `x0` is the initial state and `dt0` is the initial time delta. With the last line of code, the state can be extracted at any epoch between the initial and final time, with respect to any body and frame present in the *Universe* defined by `'wrt_Body'` and `'Frame'`.

*Propagator* belongs to the *Model* library and can be used to propagate different quantities other than the state, as in the *Trajectory* class. This method is more articulated with respect to the previous one, but more adaptable to user needs since manoeuvre and mass propagation can be added. The implementation can be divided into different steps: creation of frames and points, input definition and propagator formulation. A code example is reported to display the main steps previously reported.

```
# Add frame and point
fra = uni.frames
icrf = fra.axesId('ICRF')
earth = fra.pointId('Earth')
SC_point = fra.addPoint('Spacecraft', tempo.TimeScale.TDB)
# Set up the input
propPoint = prop.PropagatorPoint(fra, icrf, SC_point)
input = [prop.PointInput(propPoint, earth, x0, dyn, tol, tol)]
# Create the propagator
pro = prop.Propagator('Prop', t0, dt0, input)
pro.compute(tf, False)
```

The dynamic used in `input` can be defined externally in a different function or directly extracted by the *Universe* and passed as a parameter. When computing the propagation with the command `pro.compute(tf, False)`, is possible to set the flag to `True` or `False` in case the user is interested in estimating the partials (note that this feature is present also in the *BallisticPropagator*).

In all three method is possible to select different integration methods, the available algorithms are 8<sup>th</sup> order Runge Kutta schemes with four different type of interpolation and

Adams algorithm with variable order and step size; the one used to develop this work is the default method Runge Kutta Verner787 algorithm.

**Autodif:** GODOT support through this library automatic differentiation, making the computation of gradients of any function with respect to any variable trivial. *Autodif* defines a new type of object characterized by the value of the variable and the leaf, that for simplicity can be thought as a space in which the partial derivatives are stored. The parameters defined using the Automatic Differentiation library can have scalar, vector or matrix as value and more than one leaf. To clarify how the *Autodif* module works a simple example is reported below, where the gradients of the Cartesian state with respect to the orbital elements need to be computed [17].

```
# Orbital element definition
coe = [10000, 0, 0, 0, 0, 0]
ad_coe = ad.Vector(coe, 'coe')
# Conversion to cartesian element
ad_state = astro.cartFromKep(ad_coe, GM_Earth)
# Value and gradient extraction
state = ad_state.value()
gradient = ad_state.gradient()
```

Given an initial vector **coe** of orbital element, the object **ad\_state** contains in the method `value()`, the actual values of the state **x** in Cartesian coordinates and in the `gradient()` method, the gradient of the state with respect to the orbital elements  $\frac{\partial \mathbf{x}}{\partial \mathbf{coe}}$ .

## 3.2. PyGMO

PyGMO (Python Parallel Global Multi-objective Optimizer) is a library developed by the Advanced Concepts Team of ESA supporting many different problems and algorithms intended for computing parallel optimization of aerospace-related problems. PyGMO is capable of supporting constrained, unconstrained, single objective and multiple objective problems, making it suitable for any type of optimization [18]. Both local and global optimization algorithms are implemented in this library. The first ones limit the research of the optimal solution in a narrow area near the given initial guess, finding a local minimum or maximum depending on the problem. Global algorithms use a set of initial guesses, which are usually referred to as population, and evaluate the objective function outcome of each individual. The best guesses are extracted and slightly modified creating a new generation of individuals, which form a new population; these steps are repeated until

the termination criterion is satisfied and the individual which minimizes or maximizes the objective function is presented as the best solution.

In this section a brief general description of how to formulate an optimization is given, after which a simple implementation using PyGMO is presented for clarity. An optimization problem starts with the definition of the objective function  $f(\mathbf{x})$  which needs to be minimized or maximized; this function depends on a set of  $n$ -variables that together form a vector, usually referred to as decision vector.

$$\mathbf{x} = [x_1, x_2, \dots, x_i] \quad \text{for } i = 1, 2, \dots, n$$

A general optimization problem can be subjected to two type of constraints: inequality and equality ones indicated respectively as:

$$\begin{aligned} g_j(\mathbf{x}) &\leq 0 & \text{for } j = 1, 2, \dots, l \\ h_k(\mathbf{x}) &= 0 & \text{for } k = 1, 2, \dots, m \end{aligned}$$

where  $l$  and  $m$  represent an arbitrary number of constraints. In addition, it's possible to define upper and lower bounds acting directly on the decision vector, limiting the search region of the problem. Therefore, the general statement of an optimization problem subjected to inequality and equality constraints and bounds can be summarized as follow:

$$\begin{aligned} &\text{Find} && \mathbf{x} = [x_1, x_2, \dots, x_i] \\ &\text{subject to} && \begin{cases} g_j(\mathbf{x}) \leq 0 \\ h_k(\mathbf{x}) = 0 \\ \mathbf{x}^l \leq \mathbf{x} \leq \mathbf{x}^u \end{cases} \\ &\text{which minimizes} && f(\mathbf{x}) \end{aligned}$$

Any vector that satisfies the constraints is called *feasible solution*, the collection of all feasible solutions is called *feasible region* and the optimization problem is solved when the vector  $\bar{\mathbf{x}}$  such that  $f(\mathbf{x}) \geq f(\bar{\mathbf{x}})$  for each feasible  $\mathbf{x}$  is found. In PyGMO it's possible to code a problem, referred to as User Defined Problem (UDP), following these steps. First of all, as an example, a simple problem formulated in a more compact way is presented.

$$\min_{x_1, x_2} f := (x_1 - 3)^2 + (x_2 - 2)^2 \quad \text{s.t.} \quad \begin{cases} g_1 := x_1^2 - x_2 - 3 \leq 0 \\ h_1 := x_2 - 1 = 0 \\ -1 \leq x_1 \leq 1 \\ -1 \leq x_2 \leq 1 \end{cases}$$

The problem can be constructed using a `class` and two mandatory methods: `fitness` and `get_bound`; in case of a more complex problem, like the one in the example, other methods need to be added, such as `get_nic` and `get_nec` that respectively represent the number of inequality and equality constraints.

```
class example_function:
    def fitness(self, x):
        obj = (x[0] - 3)^2 + (x[1] - 2)^2
        ci1 = x[0]^2 - x[1] - 3
        ce1 = x[1] - 1
        return [obj, ce1, ci1]
    def get_bounds(self):
        return ([-1]*2, [1]*2)
    def get_nic(self):
        return 1
    def get_nec(self):
        return 1
```

Once the problem is completely defined, an algorithm, that can be selected from the one available in the library or can be implemented by the user, must be selected. Each algorithm is associated with a specific type of problem that can be fully described by three properties:

- Constrained or Unconstrained
- Single or Multi-Objective
- Continuous, Integer or Mixed integer

With the properties of the problem defined the corresponding algorithm can be selected noting that PyGMO supports algorithms from other libraries such as SNOPT, SciPy, NLOPT and IPOPT. Along with the definition of the algorithm, a termination criterion must be implemented if the default ones do not satisfy the requirements of the user; the criteria are based on relative and absolute tolerance, maximum computational time and maximum number of iterations.

At last, by giving an initial guess in the case of a local optimizer or by defining an initial population for stochastic optimization the problem can be solved.

In the context of the thesis GODOT and PyGMO have been used to deal with space-related computations and optimization problems respectively. The *Universe* function is used to define the dynamic, defined by all Solar System's planets and SRP, in which

the three satellite are propagated. This method is selected to implement the RHS since is trivial to add ephemeris file to the environment, fundamental to the transfer phase defined in Section 4.3. Another key feature used from GODOT is the *Propagator* which is used to extract the states of the spacecraft at any epochs specified by *Tempo*. The great versatility of PyGMO is exploited to create UDP taking care of different parts of the problem analysing the geometry of the formation during the operational phase and the costs in terms of delta-Vs for the transfer phase.

# 4 | Methodology

In this section, the objective is to outline the framework in which the thesis is developed and the approaches used to solve the problem. In particular, the three research objectives defined in the introductory chapter are analysed as follows. The first step is to understand how a non-optimized formation behaves in an n-body dynamic environment with SRP perturbation, varying initial displacement angle and arm length. In addition, simple initial analyses of the transfer are made to have an idea of the magnitude of characteristic parameters such as  $\Delta V$  and time of flight. Then the chapter develops by focusing on the optimization of the science phase, followed by a presentation of different transfer strategies.

## 4.1. Preliminary cartwheel analysis

The aim of the thesis is to find optimal initial conditions for the three satellites in order to maintain the geometry of the formation for as long as possible and minimize the amount of fuel needed to transfer the fleet into EDHO. The idea of tuning the conditions defining the beginning of the science phase is essential since it exploits the natural evolution of the three satellite orbits minimizing the cost of station keeping and increasing the life span of the mission. The quality and stability of the formation is defined by its geometrical characteristics, arm length ( $L$ ), arm length rate ( $\dot{L}$ ), and corner angle ( $\alpha$ ). The optimization must be carried on simultaneously for all the units of the fleet since  $L$ ,  $\dot{L}$ , and  $\alpha$  are all quantities that can be computed knowing the states of all the satellites at the same time. In the RHS defining the dynamic of the satellites the following bodies and perturbations are considered:

- Main bodies in the Solar System (Sun, Mercury, Venus, Earth, Moon, Mars, Jupiter and Saturn)
- SRP
- Neither Earth's  $J_2$  perturbation nor Sun's one are considered due to the irrelevant influence with respect to the other accelerations

The choice of considering only these perturbations comes from a simple analysis of the accelerations affecting a satellite in an EDHO. In the considered Solar System the orbits are all circular with radii equal to the semi-major axis and all planets, except Earth, are aligned with the test satellite as shown in Fig. 4.1. Since an EDHO must be considered, the Earth and the Moon are displaced by an angle  $\theta_0$  which is varied in order to compute the intensity of the gravitational acceleration as a function of different initial displacement angles. Regarding the other planets two different configurations can be identified: one in which the satellite and the planet are the closest as in Fig. 4.1 and one in which the planet is on the opposite side with respect to the Sun affecting the motion of the satellite the least. These two solutions are then merged to compute the average acceleration of the planets resulting in a constant trend as a function of  $\theta_0$  as shown in Fig. 4.2<sup>1</sup>. It can be noticed that other than the Sun which is the main attractor, the gravitational accelerations of Jupiter and Venus have a similar magnitude which can be more or less than the one of Earth depending on the  $\theta_0$ . Earth remains still the main source of perturbation since the distance between the satellite and the planet is almost constant, meaning that the gravitational pull acts continuously with the same magnitude on the spacecraft's dynamic. This is not valid for all the other planets since the condition of the closest approach is reached only once a year. The last planet considered is Mercury and any perturbation below its value, like Uranus, Neptune and the  $J_2$  accelerations are considered negligible as shown in Fig. 4.2b.

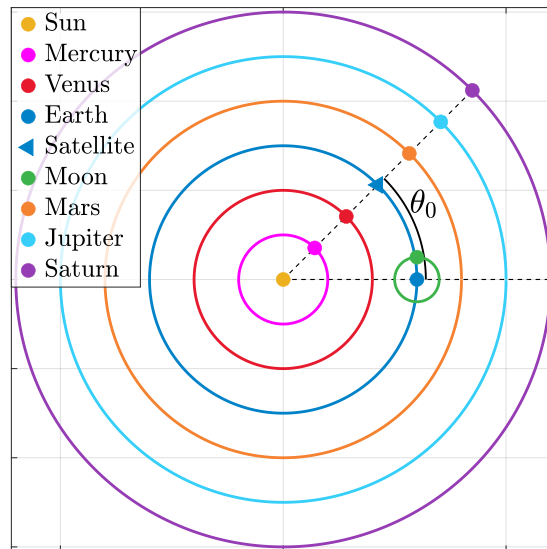
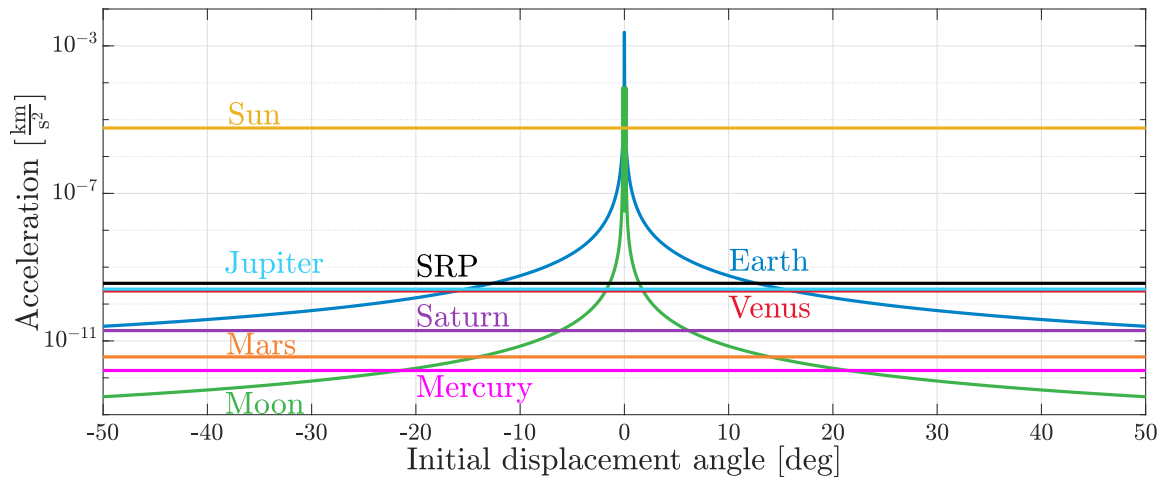


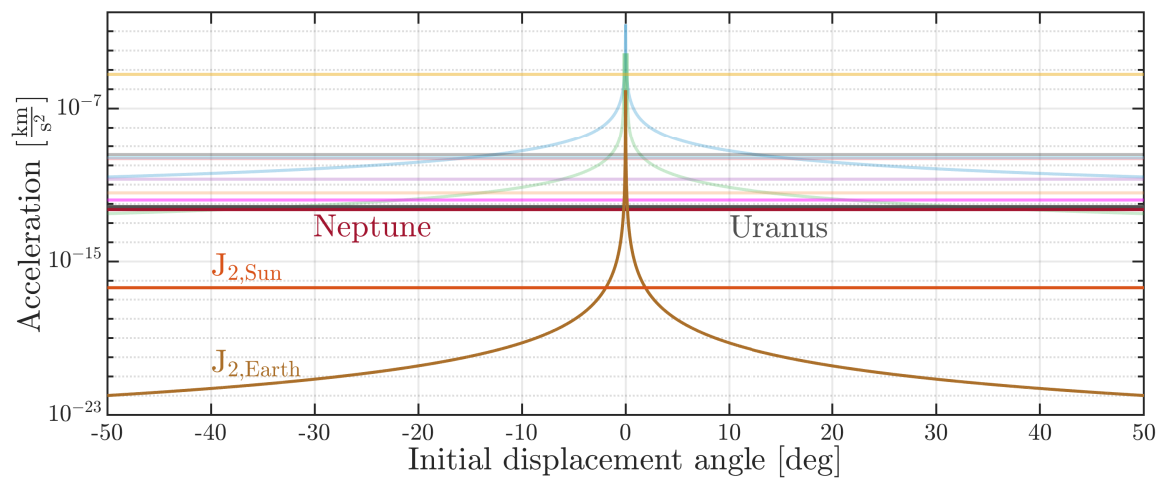
Figure 4.1: Solar System configuration for the acceleration analysis (not in scale).

<sup>1</sup>Even though two different configurations are considered the average is quite similar to the acceleration of the closest approach since the perturbations computed when the planets are further away are almost negligible.

The intensity of the SRP perturbation is one of the most relevant, meaning that a more generalized analysis of the cartwheel formation which considers all acceleration is needed. This simplified analysis gives approximate information on the order of magnitude of the most relevant perturbation defining the accelerations that must be considered to propagate the spacecraft.



(a) Considered perturbations.



(b) Neglected perturbations.

Figure 4.2: Acceleration analysis considering gravitational, SRP and  $J_2$  perturbations.

The satellites composing the fleet are somehow connected during their entire operational life, from the launch on the same carrier rocket to the operational phase in which the formation is obtained, meaning that some simplifications need to be adopted to solve the problem. First of all the entire mission is divided into two parts: the transfer phase, starting from a parking orbit around Earth and the scientific phase which begins once the formation is completely acquired. Both need to be optimized and conceiving a single

optimization problem taking care of the entire mission wouldn't be a reliable first step. Therefore, the problem is divided in two and each part can be addressed and optimized separately, keeping in mind that these segments rely on each other; the transfer must be designed to accommodate the requirements of the formation in terms of position with respect to Earth and inter-satellite distance.

#### 4.1.1. Formation analysis

In this section the behaviour of the non-optimized formation is analysed starting from the orbital elements presented in Table 2.1, which have four degrees of freedom: arm length,  $L$ , argument of perigee,  $\omega$ , right ascension of the ascending node,  $\Omega$  and the initial displacement angle,  $\theta_0$ . The latter is computed using the Mean Earth, a fictitious Earth with the same orbital period as the true one which covers a circular paths around the Sun. On a practical level, the Mean Earth is obtained by extracting at a given epoch the state of the True Earth from the ephemeris and converting the state into orbital elements. From these elements is possible to define the *osculating* orbit which is the Keplerian trajectory that the body would follow if in that instant all perturbations would vanish; every point on the perturbed trajectory has its own osculating orbit. The Mean trajectory has the same plane and period as the osculating one, but it follows a circular orbit, meaning that only the eccentricity from the initial orbital elements must be modified and set to zero. These three different orbits are shown in Fig. 4.3 considering a one year propagation. The difference between the Osculating and Mean Earth is small in terms of trajectory, but the key factor which differentiate these two orbits is that Mean Earth follow a circular path. Let's analyse the geometry characteristics using a Keplerian model with arm length of  $2.5e6$  km, an initial displacement angle of  $-20^\circ$  and a counter clock-wise rotation in which only the Sun affects the motion of the satellites.

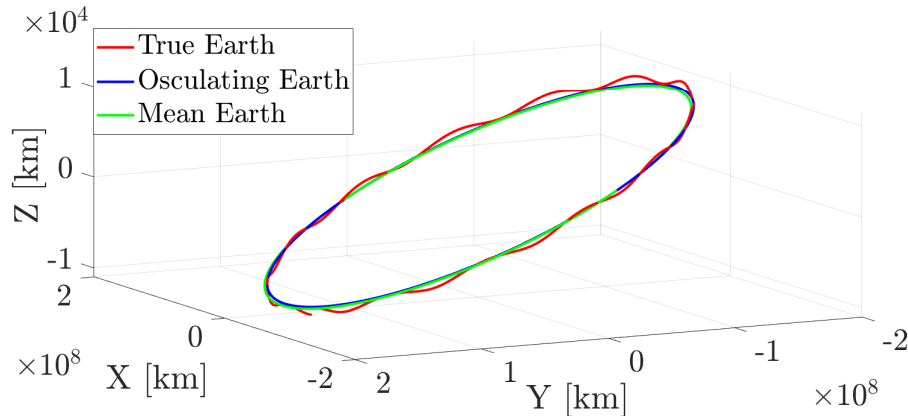


Figure 4.3: Difference between True, Osculating and Mean Earth.

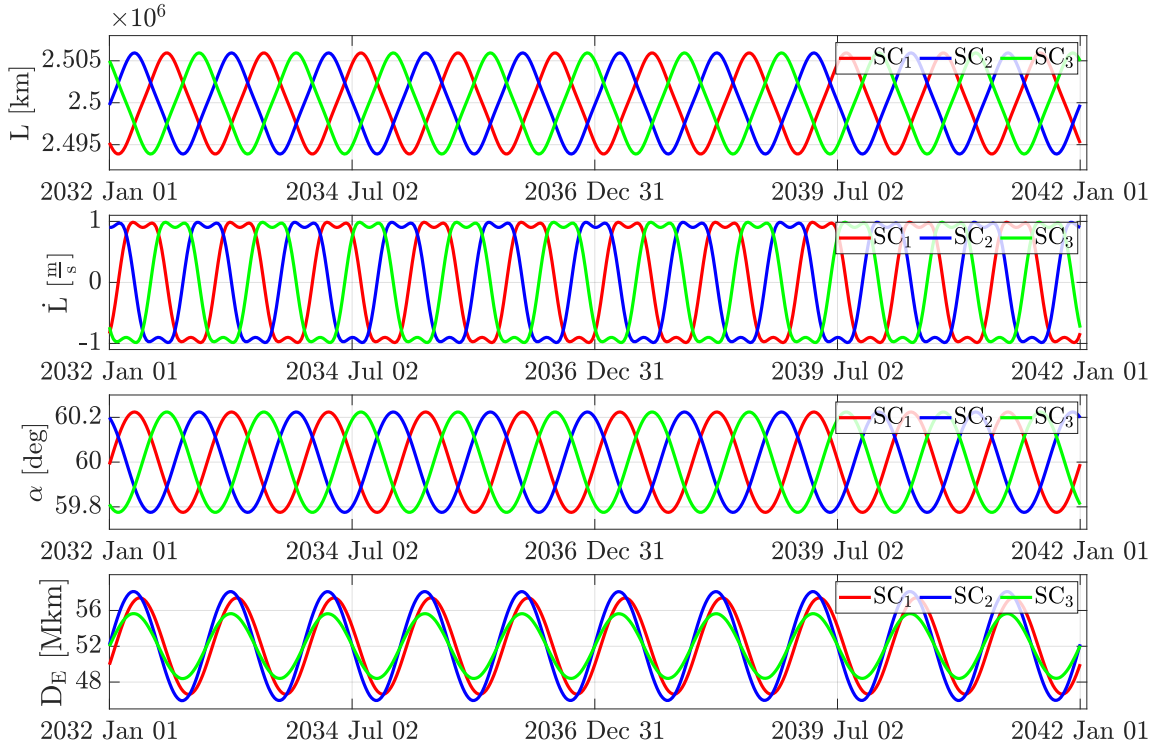


Figure 4.4: Geometry evolution in Keplerian model.

The orbital elements presented in Table 2.1 are propagated for 10 years and the geometric characteristics and the distance from the True Earth are computed. As can be seen in Fig. 4.4, the geometry is not frozen and the values of  $L$ ,  $\dot{L}$  and  $\alpha$  are not constant in time; the flexing of the formation is usually referred to as *breathing* and is due to the fact that the orbital elements are the results of a linearization, valid only for near-circular chief orbits and small relative orbit's radius compared to the inertial one, which is then used in a non-linear environment. The last condition is not well satisfied since considering an equilateral triangle of side  $a$  the distance between the centre and the vertex is  $a/\sqrt{3}$ , meaning that the ratio between the semi-major axis and chief-deputy distance is 0.965% for a nominal arm length of  $2.5e6$  km, which is not negligible. In addition, the linearised dynamics that would generate a GCO with a constant distance between the satellites and the centre of the formation, is used in a n-body environment causing the distance to the centre to vary with a one-year periodicity [19].

The next step consists in propagating the satellites in a complete dynamical environment taking into account all the perturbations. The main perturbation is due to Earth which accelerate constantly the satellites in a near along-track direction; this acceleration generates a drift in the semi-major axis, which translates into an increment or reduction of the distance between Earth and the fleet, depending if the formation is trailing or leading.

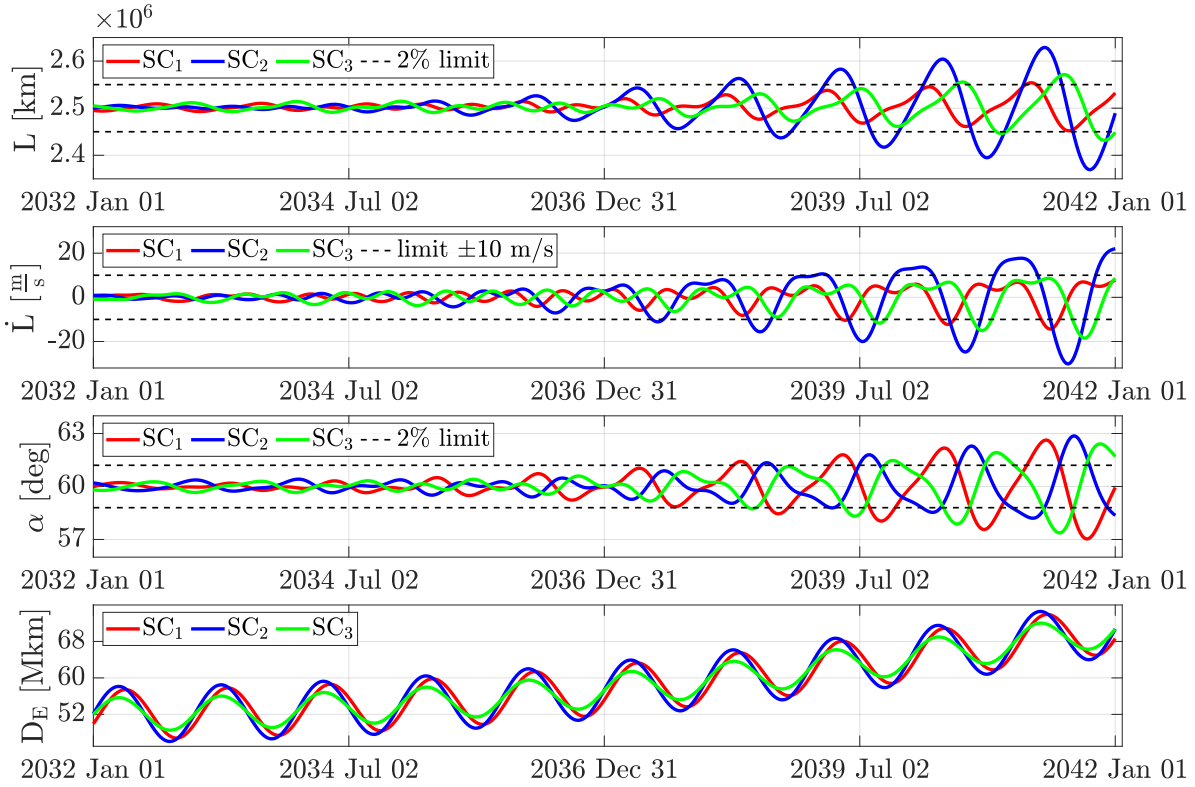


Figure 4.5: Geometry evolution in N-body model.

For a trailing formation, the Earth-Moon system accelerates the satellites along the velocity direction which increases the semi-major axis, resulting in a lower orbital period. With these conditions the formation drifts backwards, increasing the distance from Earth as can be seen in Fig. 4.5. The addition of these perturbations makes the geometrical parameters diverge from the nominal conditions, generating an unstable configuration capable of threatening the science requirements. It is necessary to impose some requirements on  $L$ ,  $\dot{L}$  and  $\alpha$  to verify a posteriori if the optimization technique can satisfy such limits; in this case a 2% bound for arm length and corner angle and  $\pm 10$  m/s limit of arm length rate are considered, which correspond to slightly less rigid constraints with respect to the one of LISA. Neither of these requirements is satisfied for the time period considered meaning that an optimization of the initial conditions is necessary.

|                  | $L$ [km]                                 | $\dot{L}$ [m/s]   | $\alpha$ [deg]   |
|------------------|--|-------------------|------------------|
| <b>Keplerian</b> | $[2.494 \times 10^6, 2.506 \times 10^6]$ | $[-0.98, 0.98]$   | $[59.78, 60.22]$ |
| <b>N-body</b>    | $[2.370 \times 10^6, 2.629 \times 10^6]$ | $[-30.17, 22.04]$ | $[57.03, 62.87]$ |

Table 4.1: Min and max deviation of  $L$ ,  $\dot{L}$  and  $\alpha$  in Keplerian and N-body model.

The next step consists in analysing the behaviour of the formation by varying the parameters that define its geometry and position. The main focus is on the arm length and the initial displacement angle since a variation of  $\omega$  modifies the rotation direction seen from the Sun and  $\Omega$  results only in a relative rotation of the geometry around its centre. Not all initial displacement angles are acceptable since by getting too close to Earth the gravitational perturbation would be too strong for the formation to keep its geometry; therefore, the analysis is limited to an initial angle higher than  $\pm 10^\circ$ . By increasing the angle, the distance from Earth increases as well, decreasing the overall perturbations and making the configuration more stable; this can be shown by propagating the initial conditions considering different values of the initial angle  $\theta_0$  and evaluating the maximum deviation of each geometrical parameters. The maximum and minimum value of  $L$ ,  $\dot{L}$  and  $\alpha$  at different initial displacement angles are shown in Fig. 4.6 which displays a clear instability with increasingly higher variations for configurations closer to Earth.

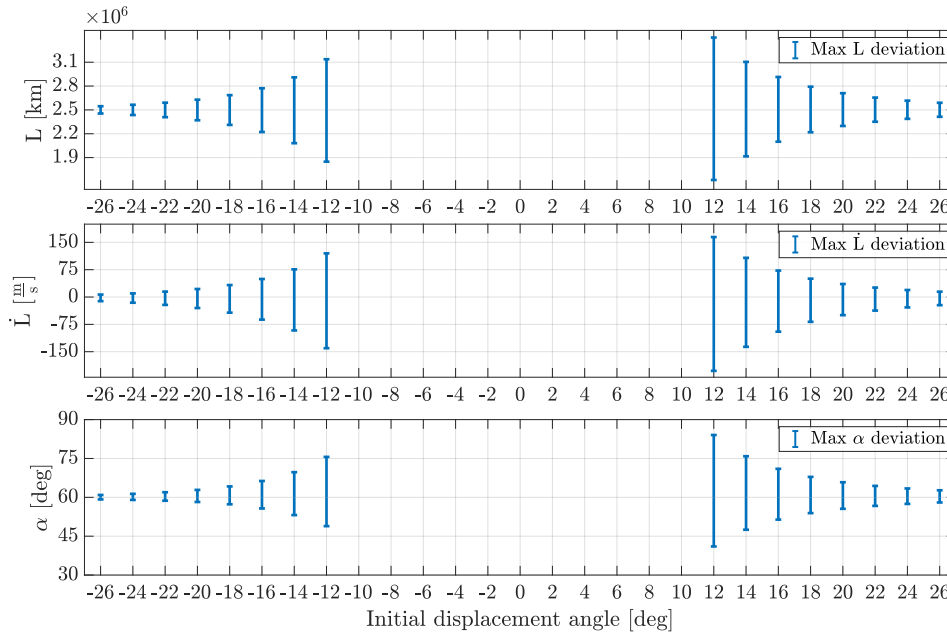


Figure 4.6: Geometry parameters in function of the initial displacement angle.

A similar analysis can be done for arm length variations considering a wide range between  $1e4$  km and  $2e7$  km to catch a particular trend as shown in Fig. 4.7. The maximum deviation of  $L$  and  $\dot{L}$  increases by increasing the arm length since by doing so the distance from the centre raises, increasing both the *breathing* of the formation and the gravitational perturbations affecting each satellite. Regarding the corner angle, for low values of arm length the maximum deviation decreases and then returns to increase as the other

parameters for high  $L$ . These results are essential to understand the behaviour of the formation in different conditions and to build and design an optimal strategy capable of maintaining limited in time the maximum deviation of each geometric characteristic.

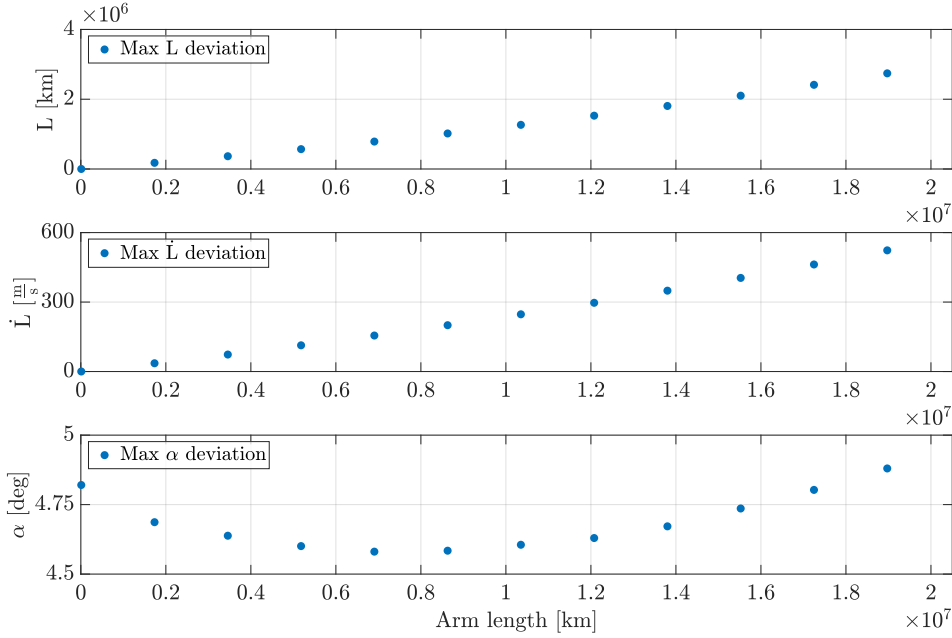


Figure 4.7: Geometry parameters in function of arm length.

The last considerations on the evolution of the formation can be done by analysing the orbital elements in the ecliptic frame. As previously discussed for trailing cartwheel formation the semi-major axis increases in time, while eccentricity, inclination and argument of perigee all starting from the same conditions evolves into different final values; the idea of the optimization consists in tuning the initial orbital elements in a way that makes the final conditions satisfy the requirements.

#### 4.1.2. Transfer analysis

The fleet can be transferred from Earth towards Earth-Displaced Heliocentric Orbit with different strategies that can be divided into such categories [20]:

- a) Direct transfer with or without Deep Space Manoeuvres (DSM), in which the satellites are injected on a transfer trajectory towards the final orbit directly by a launch vehicle.
- b) Trajectory considering a transfer module that from an Earth-bounded orbit reaches the escape condition thanks to an Apogee Raising Manoeuvre (ARM) which increases the apogee with multiple manoeuvres, as was done for the LISA Pathfinder mission [21].

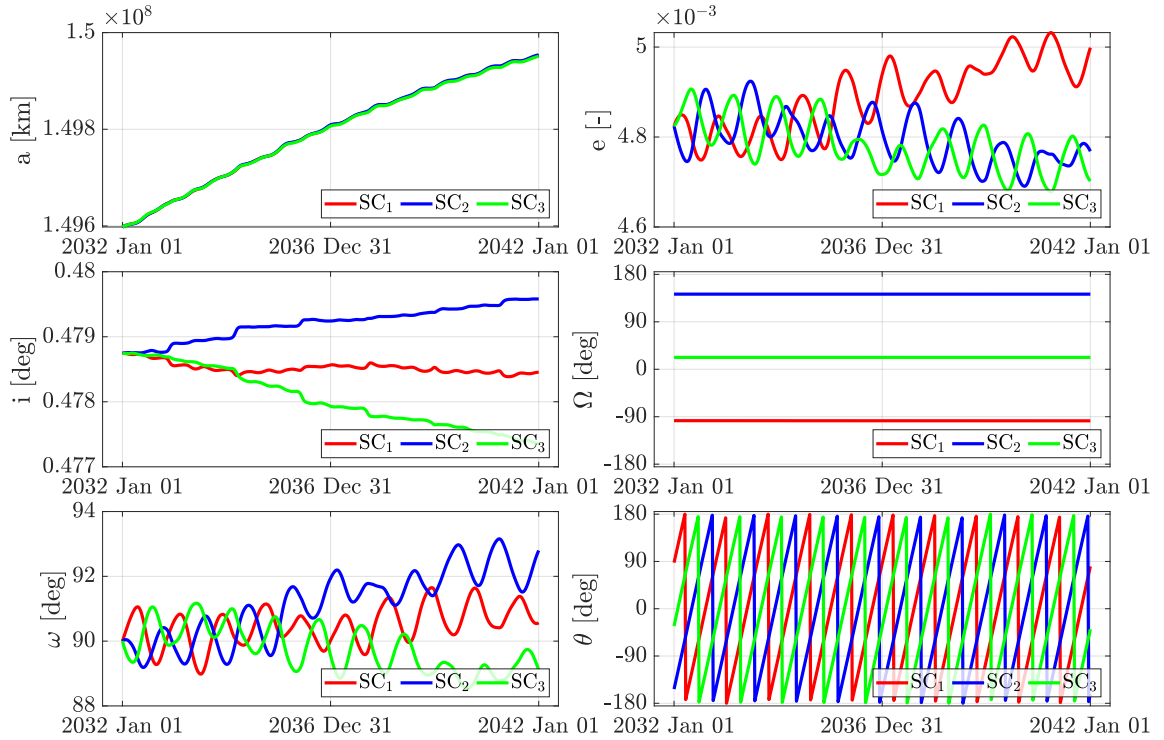


Figure 4.8: Orbital elements evolution.

- c) Low-energy transfer such as escaping Earth using an unstable manifold in the Sun-Earth system or Lunar Gravity Assist (LGA).

The problem of transferring a satellite from Earth to a general EDHO can be thought of as a phasing manoeuvre with a small plane change due to the different inclinations of the final orbits. The direct injection strategy can be pursued only in case a powerful launcher is available and the satellites can be put directly from Earth in an escape trajectory; the other options are possible alternatives in case smaller launchers, not capable of reaching the escape velocity, are used. This work is intended as a preliminary mission analysis and for this reason the transfer is based on a direct injection without DSM. The first approach to the transfer design is simple Lambert problem from Earth targeting an EDHO with an initial displacement angle of  $-20^\circ$ . To solve the Lambert problem an initial and final positions are needed: in this case the True Earth is used for departure, while the arrival orbits are the ones optimized with the methods presented in Section 4.2. Multi-revolution Lambert problems are not presented as an available solution due to a limit in the maximum transfer time, imposed to avoid high commissioning time. As can be seen in Fig. 4.9 the time of flight for each spacecraft is in the order of 360 days, while the values of  $\Delta V$  have a minimum around 1.2 km/s. The trend shown in the plot is repeated each year, while it can be noticed that a seasonal variation of  $\Delta V$  occurs with two local minima

obtained departing in April/May and in October/November. In Table 4.2 the results of leading and trailing configurations for different initial displacement angles are presented. The minimum  $\Delta V$  for leading orbits is found later in the year, in the October/November period, and the cost is higher with respect to ETHO since lowering the perihelion to obtain ELHO is more expensive than increasing the aphelion by the same quantity[20].

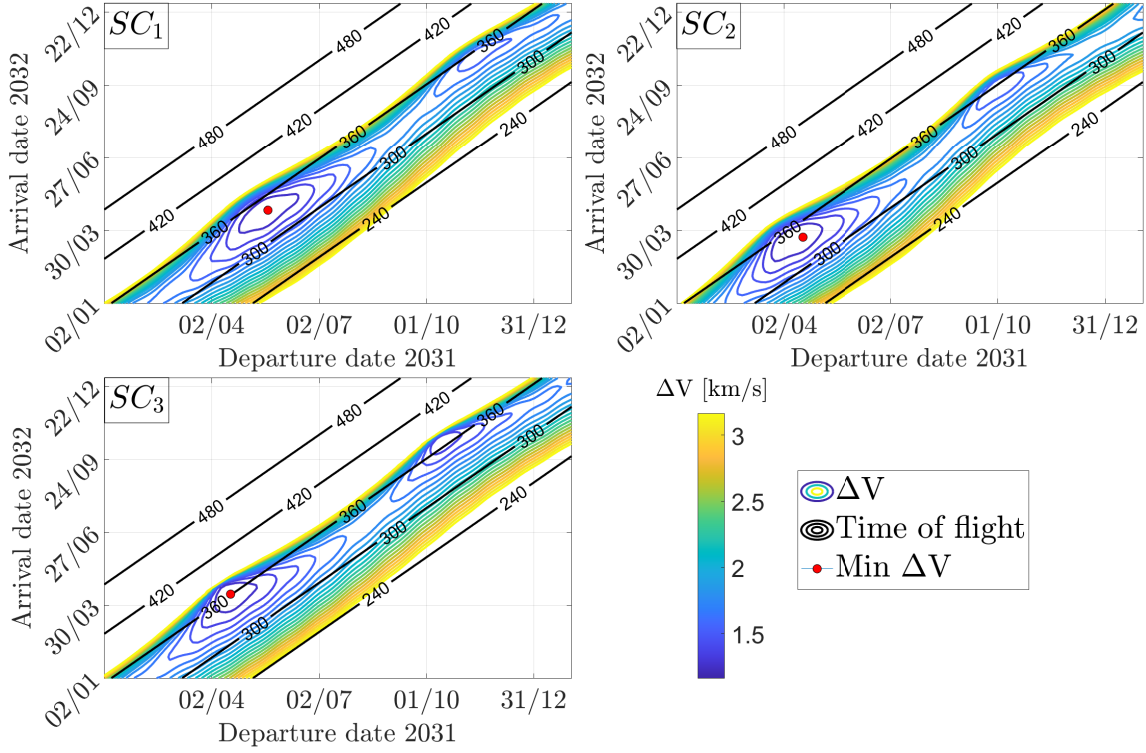


Figure 4.9: Pork-chop opportunity maps for each satellite.

The transfer is far more complex than a simple Lambert problem since the three satellites need to be launched all together using a single launch vehicle meaning that all the trajectory are somehow connected. The different design strategies proposed to transfer the fleet will consider only trailing formations due to lower cost in terms of  $\Delta V$ .

|                        | $\Delta V_1$ [km/s] | $\Delta V_2$ [km/s] | $\Delta V_3$ [km/s] | Period           |
|------------------------|---------------------|---------------------|---------------------|------------------|
| $\theta_0 = -20^\circ$ | 1.29                | 1.26                | 1.16                | April/May        |
| $\theta_0 = -15^\circ$ | 1.03                | 1.00                | 0.91                | April/May        |
| $\theta_0 = 15^\circ$  | 1.09                | 1.07                | 0.97                | October/November |
| $\theta_0 = 20^\circ$  | 1.41                | 1.38                | 1.28                | October/November |

Table 4.2: Cost and period of the transfer for different  $\theta_0$ .

## 4.2. Science phase

In this section different optimization techniques to maintain the formation stable are presented. The idea is to tune the initial orbital elements to satisfy the requirements imposed on the geometry of the formation. The first step is to identify the decision vector which is defined by an initial time, corresponding to the moment that the fleet acquires the geometry, and three sets of orbital elements, fully defining the initial conditions of the formation.

$$\mathbf{y} = \{t_0, \mathcal{K}_1, \mathcal{K}_2, \mathcal{K}_3\} \quad \text{where } \mathcal{K}_j = \{a, e, i, \omega, \Omega, \theta\} \quad \text{with } j = 1, 2, 3$$

With the decision vector well designed a cost function  $J$  minimizing the perturbation must be defined with the idea of incrementing its value every time the geometry exceeds or moves towards the geometrical bounds. To build such a cost function two different approaches can be used. In the first one, a penalty is added every time a constraints' violation is detected; since the objective is to limit the range between the maximum and minimum value of  $L$ ,  $\dot{L}$  and  $\alpha$ , each of this parameter has an upper and lower limit that, if infringed, would add a penalty to the cost function [16]. This concept is repeated at each instant of time between  $t_0$  and the final time, for each of the geometrical parameters. The problem with such formulation is that the gradient of the cost function with respect to the decision vector is not well defined since the  $J$  itself is not continuous in time.

The second approach consists in defining a continuous cost function which penalizes the difference between the geometrical parameters. By focusing on the geometry of a triangle, the minimization of the difference between its sides would push the triangle towards an equilateral formation, resulting in no relative velocity between the vertex and angles of  $60^\circ$ . The same can be obtained if the difference of the relative velocities is minimized since the formation will move towards an equilateral triangle geometry as well; note that if the same reasoning is applied to a cost function based only on the corner angles, it would be less reliable since constraining only the angles does not impose any restriction on the *breathing* motion of the formation. This leads to the definition of the following costs functions:

$$J_{Length} = \int_{t_0}^{t_f} (L_1(t) - L_2(t))^2 + (L_1(t) - L_3(t))^2 dt$$

$$J_{Rate} = \int_{t_0}^{t_f} (\dot{L}_1(t) - \dot{L}_2(t))^2 + (\dot{L}_1(t) - \dot{L}_3(t))^2 dt$$

The cost functions do not contain the difference between elements  $(\cdot)_2$  and  $(\cdot)_3$  since it would be redundant due to transitive property defining an implicit relation between these parameters. The final optimization problem consists in minimizing  $J_{\text{Length}}$  or  $J_{\text{Rate}}$  with respect to  $\mathbf{y}$  without any equality or inequality constraints.

The optimization procedure is computed following these steps which are the same for the two cost functions.

**Initial guess:** The initial guess must be retrieved by defining the initial displacement angle  $\theta_0$ , the arm length,  $L$  and the initial time  $t_0$  which is used to define the longitude of the Mean Earth  $l_{\text{ME}}$  and the mean anomaly of each satellite. Then, the three sets of initial orbital elements are converted into initial Cartesian states composed of positions and velocities.

**Propagation:** The geometrical parameters are computed from  $t_0$  to  $t_f$ , meaning that the initial state of the satellites must be propagated as well. A time grid is defined and by calculating the state at each time also the geometry can be calculated. For  $J_{\text{Length}}$  only the arm length is needed to compute the cost function, while for  $J_{\text{Rate}}$  both  $\dot{L}$  and  $L$  are necessary.

**Compute the cost function:** At this point the values of  $L$  or  $\dot{L}$  are available at each time defined in the grid, making possible the computation of the cost functions. Since the algorithm used for this optimization is a gradient-based algorithm the gradient of  $J$  with respect to  $\mathbf{y}$  need to be computed.

$$\frac{\partial J}{\partial \mathbf{y}} = \left[ \frac{\partial J}{\partial t_0}, \left( \frac{\partial J}{\partial a_j}, \frac{\partial J}{\partial e_j}, \frac{\partial J}{\partial i_j}, \frac{\partial J}{\partial \omega_j}, \frac{\partial J}{\partial \Omega_j}, \frac{\partial J}{\partial \theta_j} \right)_{j=1,2,3} \right]$$

By running the optimization problem is possible to retrieve the optimized initial time and orbital elements. From these quantities the final trajectories defining a stable formation are calculated and collected into OEM (Orbit Ephemeris Message). This type of format contains position and velocity of a single spacecraft in a time interval defined by an initial and final epoch. This format is the recommended standard by the CCSDS to store ephemeris data and in this work is obtained by the mean of the SPICE utility *spk2oem*. Building ephemeris files for each optimized trajectory will come in handy during the presentation of the optimization of the transfer strategies in Section 4.3.

The process is the same for the two cost functions and will be used to optimise different configurations of the cartwheel varying  $\theta_0$  and  $L$  to identify which  $J$  is more suitable for

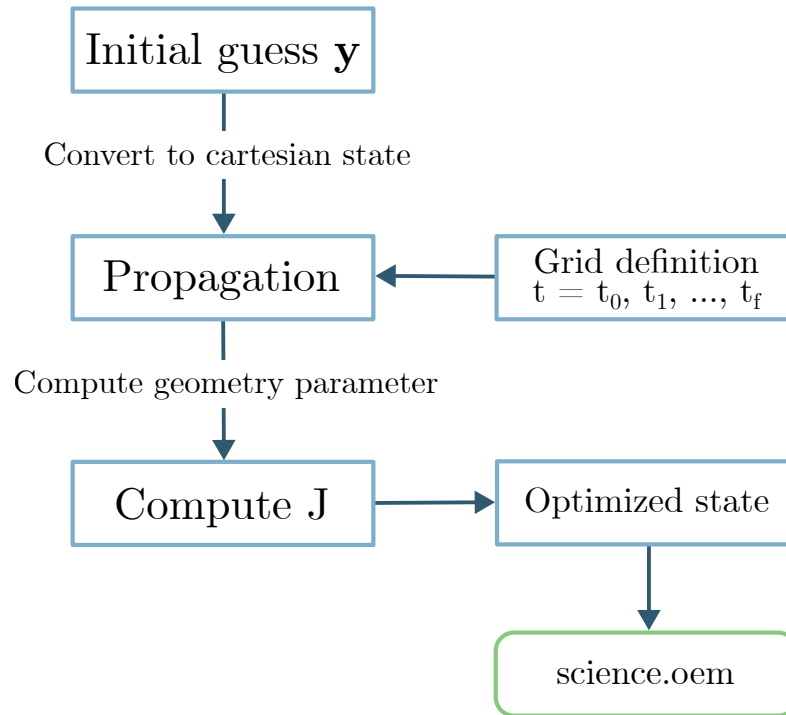


Figure 4.10: Diagram showing the steps followed to optimize the scientific phase.

this problem. The whole process used to optimize the formation maintenance is briefly summarized in the diagram presented in Fig. 4.10.

### 4.3. Transfer phase

In this section two different strategies to transfer, within reasonable  $\Delta V$  and time of flight, the fleet from Earth to the final science orbits will be presented considering a direct injection, meaning that the launcher selected must be capable of reaching the escape velocity. The transfer problem can be simplified by splitting the trajectory into two parts: a hyperbolic escape from a parking orbit up to the Earth's Sphere of Influence (SOI) and a heliocentric transfer from the SOI to the final science orbit defined by the OEM files computed in Section 4.2. The idea is to optimise the manoeuvres and the conditions at infinite (equivalent to the conditions at the SOI) in such a way that the heliocentric transfer and the hyperbolic escape can be obtained by propagating forward and backward the initial conditions. The infinite velocity  $\mathbf{v}_\infty$  is defined by the magnitude  $v_\infty$ , the infinite right ascension  $\alpha_\infty$  and the infinite declination  $\delta_\infty$  as shown in Fig. 4.11. The position on the sphere of influence is not subjected to an optimization since it can be defined from  $\mathbf{v}_\infty$  by fixing the perigee and the inclination of the departing hyperbola. For formation flying missions the spacecraft are usually launched with a single rocket;

therefore, both strategies consider for the first segment of the trajectory a carrier hosting all three satellites. The carrier does not have a propulsion system, follows the infinite conditions of the launcher and has the possibility of releasing each spacecraft at different instants, increasing the degree of freedom of the problem. Other than optimizing the initial conditions at infinite and the time at which the spacecraft are released the problem needs to minimize the total cost of the transfer, optimizing the  $\Delta V$  of the manoeuvres.

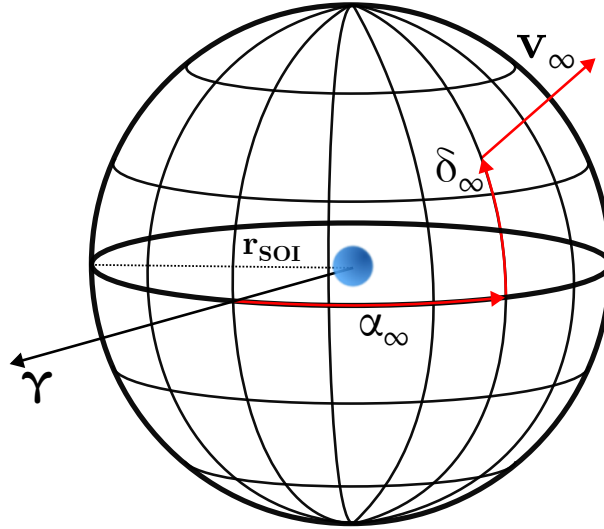


Figure 4.11: Condition at infinite defined by  $v_\infty$ ,  $\alpha_\infty$  and  $\delta_\infty$ .

### 4.3.1. First Transfer Strategy

The first strategy approaches the problem by dissecting the transfer into single trajectories in which each spacecraft is optimized individually. This is done by developing a simple single shooting method between two known trajectories defined by ephemerides: the final science orbit, already computed and stored into OEM, and the carrier trajectory, which is still unknown. The objective is to compute an acceptable carrier orbit, defined only by the condition at infinite, create an OEM file containing the relative ephemeris and then apply the single shooting method between the two known trajectories.

The entire strategy can be defined by these main steps:

1. Define the carrier orbit by optimizing singularly each satellite using Problem 1.1, in which the initial infinite conditions are optimized to minimize the final  $\Delta V$ .
2. Select the reference trajectory among the ones just optimized to be used as a carrier.
3. Reoptimize using Problem 1.2 the remaining trajectories from the carrier to the final orbit in order to obtain three complete trajectories.

Initially, the satellites are treated as three individual objects departing from the SOI with  $\mathbf{v}_\infty$  defined by the launcher; the decision vector is formed by the conditions at infinite, the initial time in which the spacecraft is on the SOI and the final time when the science orbit, indicated with  $(\cdot)^s$ , is reached. The cost function of such problem, defined in Problem 1.1, is composed only by the final  $\Delta V$ , since the initial  $\Delta V$  is given by the launcher and not by the propulsion system of the spacecraft. Despite this, even though the  $\mathbf{v}_\infty$  is not directly included in the cost function, it is heavily bounded to limit its value around hundreds of m/s in order to avoid relying too much on the launcher performance. The three carrier trajectories obtained with this optimization have all different initial conditions and lead the satellites into their respective science orbits, completely independent from each other. The problem is formally stated below and graphically represented in Fig. 4.12a.

**Problem 1.1.**

|                 |   |
|-----------------|---|
| Find            | $\mathbf{y}_1 = [v_\infty, \alpha_\infty, \delta_\infty, t_i, t_f]$                     |
| subject to      | $\begin{cases} x(t_f) = x^s(t_f) \\ y(t_f) = y^s(t_f) \\ z(t_f) = z^s(t_f) \end{cases}$ |
| which minimizes | $\Delta V_f$  |

The selection process to choose the reference trajectory is based on the initial time; between the three optimized transfers, the earliest one is used as the carrier for all the other satellites since ideally, this trajectory will contain also the optimal releasing times of the two other units. This statement is valid only if the optimal releasing time and the time in which the satellite is on the SOI are relatively similar, which will be verified in Section 5.2.1. The reference orbit is then propagated for a limited interval and the carrier's states are computed and collected into an OEM file.

The final step consists in reoptimizing the other two satellites using a simple shooting methods departing from the carrier orbit and arriving at the final science trajectory as presented in Problem 1.2. This problem has as decision vector the releasing time  $t_i$ , the arrival time  $t_f$  and the vectorial components of the initial  $\Delta V$ , and as objective function the sum of the initial and final delta-Vs. In this case, both delta-Vs are considered since after detaching from the carrier the spacecraft needs to change the initial trajectory to reach its final arrival scientific orbit since the carrier path is optimal only for the spacecraft non-optimized with this problem. The statement of the second optimization problem and its graphical interpretation are shown respectively in Problem 1.2 and Fig. 4.12b.

**Problem 1.2.**

|                 |   |
|-----------------|---|
| Find            | $\mathbf{y}_2 = [t_i, t_f, \Delta \mathbf{V}_i]$  |
| subject to      | $\begin{cases} x(t_f) = x^s(t_f) \\ y(t_f) = y^s(t_f) \\ z(t_f) = z^s(t_f) \end{cases}$ |
| which minimizes | $\Delta V_i + \Delta V_f$   |

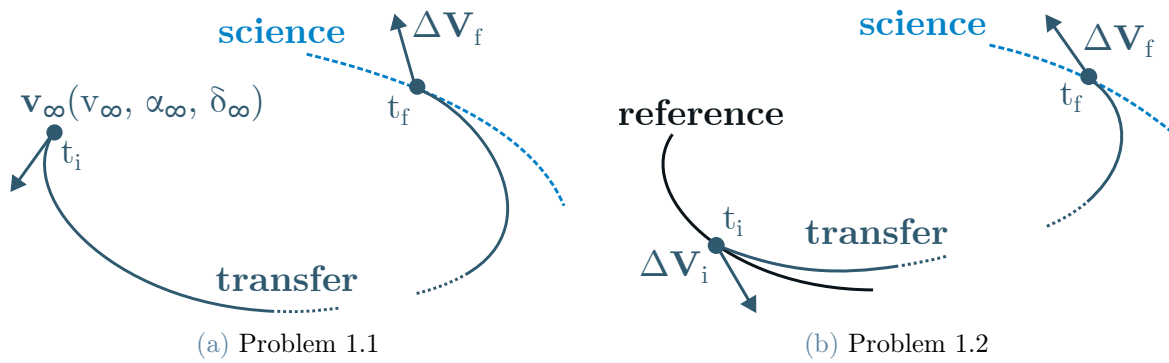


Figure 4.12: Schemes of the optimization problem for the first strategy.

The diagram in Fig. 4.13 summarizes the whole optimization process: the problem is greatly simplified by sectioning the entire transfer into individual segments that can be solved in parallel. Even though the optimizations are all carried on individually, the trajectories must be connected to each other and this issue is addressed by providing a common initial carrier trajectory. The final result considering the presence of all three satellites is shown in Fig. 4.14. In this example by solving Problem 1.1 turns out that if hypothetically the spacecraft were launched individually, the third S/C would reach the SOI first, making its trajectory the reference for the other two. The trajectory of the third spacecraft is completely defined from the first optimization process, while Problem 1.2 takes care of the trajectory of the other two satellites which were not selected as reference. The new optimized trajectories start from the carrier orbit detaching at optimal times and arrive on the final science orbit, completing the entire transfer.

This approach breaks the transfer into smaller segment in order to ease the solving process which becomes more manageable from a computational point of view. On the other hand, even though singularly the optimization problems can be computed quite fast, the downside is that five problems must be solved, three to obtain the reference trajectory and two to reoptimize the the missing satellites, making this procedure fairly long. The major disadvantage of this strategy is that the satellite injected in a heliocentric leg

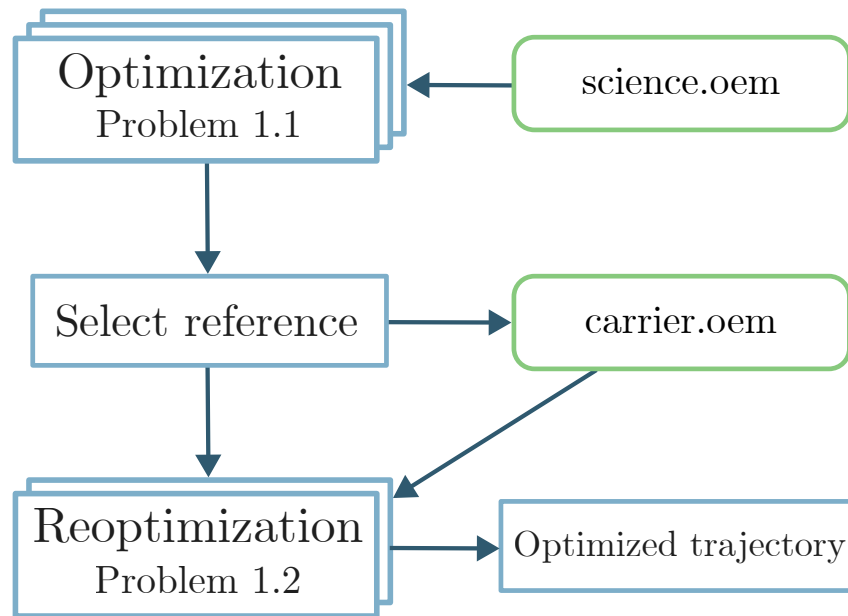


Figure 4.13: Diagram of the optimization process used for the first strategy.

directly by the launcher will always have a lower  $\Delta V$  with respect to the other since the initial  $\Delta V$  is not given by the onboard propulsion system. In a mission such as the one under analysis, in which all the satellites are identical, a different cost in  $\Delta V$  translates into different amounts of fuel remaining in the tanks. This fuel difference can limit the mission under different aspects; by following this transfer strategy two spacecraft have less fuel, meaning that a lower operational lifetime imposed by the exhaustion of propellant is expected. This phenomenon can be mitigated by forcing the satellite with more fuel to execute more frequent trajectory correction manoeuvres to compensate for the lack of manoeuvrability of the other satellites. This solution solves partially the problem of having different transfer costs between the spacecraft but increases the complexity of mission management during the operational phase.

### 4.3.2. Second Transfer Strategy

The second transfer strategy addresses the problem in a more generic way, avoiding the simplifications added in the first case such as constraining the trajectory of a satellite to follow the one of the carrier. The idea for this transfer is to optimize the conditions at infinite defined by  $\mathbf{v}_\infty$  and then consider three distinct releasing times, one for each spacecraft. As a consequence, the infinite conditions are so to be optimal for all three satellites and not just for a single spacecraft, meaning that the total  $\Delta V$  budget of the transfer is distributed more evenly between the units of the fleet.

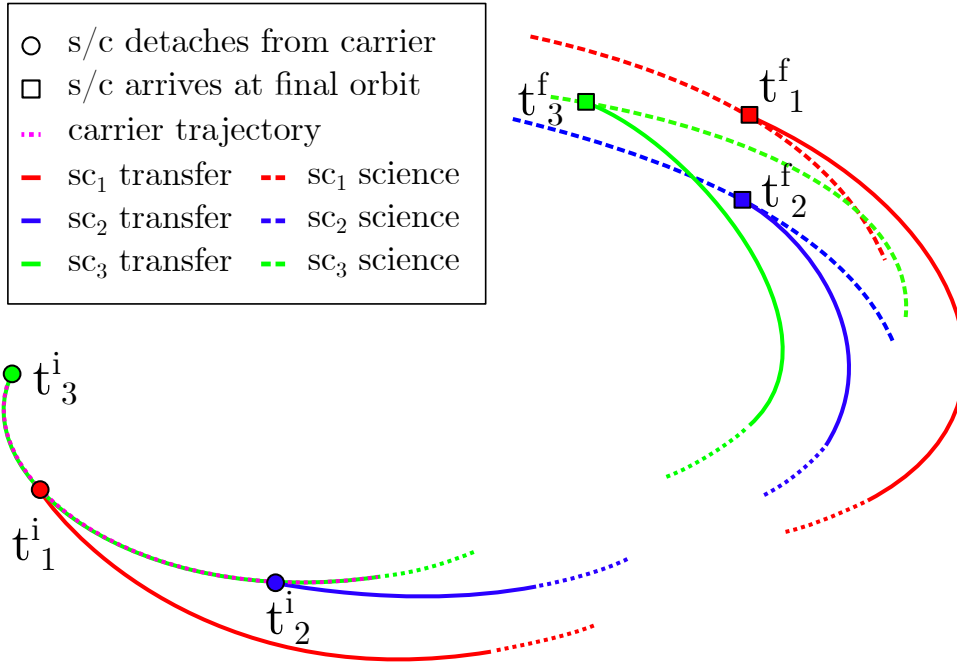


Figure 4.14: Resulting trajectories for the first optimal transfer strategy.

The strategy is briefly summarized in Fig. 4.15 and follows these steps:

1. Define the initial conditions of the carrier and propagate its trajectory.
2. Extract the initial conditions of each satellite from the state of the carrier and propagate the trajectories up to the final time.
3. Compute the cost function and the constraints with the final conditions of the satellites and obtain the three optimized transfer trajectories.

The first phase consists in defining the trajectory of the carrier, indicated with  $(\cdot)^c$ , using the initial conditions  $(v_\infty, \alpha_\infty, \delta_\infty)$  and an initial and final time, respectively  $t_0$  and  $t_f$ . The initial and final times are needed to propagate the carrier's orbit from which the initial states of the satellites are extracted; these are not optimization variables, meaning that the optimal transfer trajectory of each spacecraft is bounded to start after  $t_0$ , decreasing the search space of the problem. Once the carrier's trajectory is computed, it is possible to extract the initial state at the releasing time of each satellite; the positions are given by the position of the carrier and velocities by the velocity of the carrier plus the initial  $\Delta V_i$ . The next step consists in propagating the trajectories of the satellites up to the final times and computing the remaining part of the cost function, the final delta-Vs, and the constraints on the final positions. With this information the optimization problem stated in Problem 2 is fully described and can be solved obtaining the optimized transfer trajectories.

## Problem 2.

|                 |   |
|-----------------|---|
| Find            | $\mathbf{y}_3 = [v_\infty, \alpha_\infty, \delta_\infty, \boldsymbol{\chi}_1, \boldsymbol{\chi}_2, \boldsymbol{\chi}_3]$                                  |
| subject to      | $\begin{cases} \mathbf{r}_1(t_f) = \mathbf{r}_1^s(t_f) \\ \mathbf{r}_2(t_f) = \mathbf{r}_2^s(t_f) \\ \mathbf{r}_3(t_f) = \mathbf{r}_3^s(t_f) \end{cases}$ |
| which minimizes | $\Delta V_1 + \Delta V_2 + \Delta V_3$  |
|                 | $\boldsymbol{\chi}_1 = [t_{1,i}, t_{1,f}, \Delta \mathbf{V}_{1,i}]$   |
|                 | $\boldsymbol{\chi}_2 = [t_{2,i}, t_{2,f}, \Delta \mathbf{V}_{2,i}]$   |
|                 | $\boldsymbol{\chi}_3 = [t_{3,i}, t_{3,f}, \Delta \mathbf{V}_{3,i}]$   |
| where           | $\Delta V_1 = \Delta V_{1,i} + \Delta V_{1,f}$  |
|                 | $\Delta V_2 = \Delta V_{2,i} + \Delta V_{2,f}$  |
|                 | $\Delta V_3 = \Delta V_{3,i} + \Delta V_{3,f}$  |

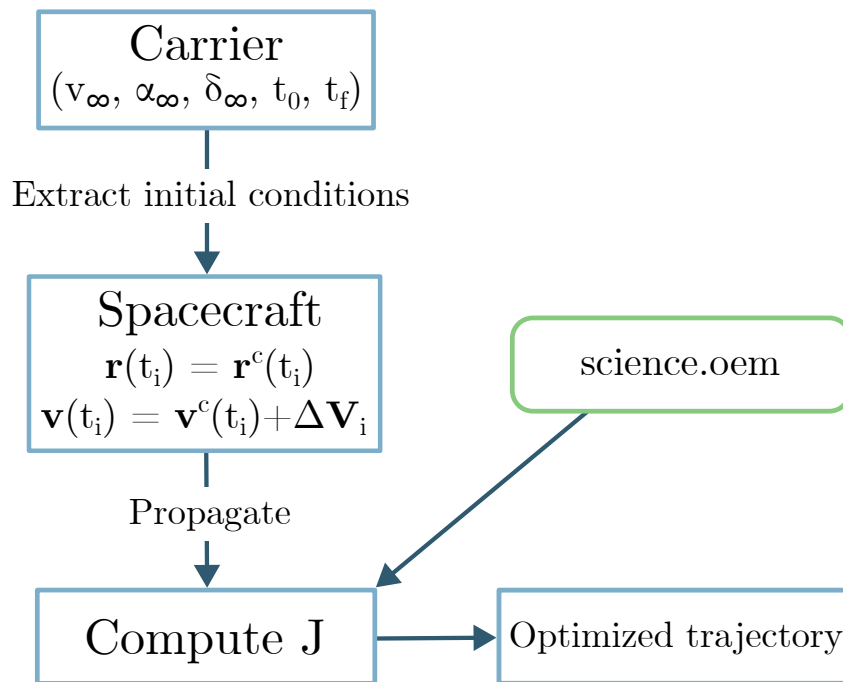


Figure 4.15: Resulting trajectories for the second optimal transfer strategy.

As can be seen in Fig. 4.16 the carrier has its own trajectory and each satellite is released individually at a different time. As mentioned before, the time when the carrier and all the satellites reach infinite conditions is fixed, optimizing only the releasing times. The search space is further limited by imposing that the three satellites have maximum one month after  $t_0$  to detach from the carrier and start their journey toward the final orbit. The

selected time range is completely arbitrary, but it seemed reasonable to allow significant freedom in this sense, recalling that the expected time of flight is one year.

The main disadvantage of this strategy is that is computationally heavier than the one described in Section 4.3.1 since the optimization problem has to define the optimal values of 19 variables; although the search space for time is limited to one month and all the variables are bounded, the space defined by the feasible solutions is still massive. By stating the problem in this way the major disadvantage of having delta-Vs with different values is partially eliminated since all satellites have both an initial and final  $\Delta V$ . It is not excluded that with this strategy the carrier injects the three satellites into a heliocentric orbit which is more favourable in terms of  $\Delta V$  to one S/C with respect to another. However, compared to the first strategy in which this phenomenon is embedded into the problem since one spacecraft always performs one less manoeuvre, this case largely averts this issue and its presence is not consistent as proved by the results in Section 5.2.2. Finally, having a similar amount of fuel in all satellites allows having a more balanced allocation of correction manoeuvres between the units of the fleet and manages to eliminate the different operational lifetimes due to the lack of propellant. This is undoubtedly the best and most promising strategy and it will be analysed more extensively in Chapter 5, completely dedicated to the results of the optimizations.

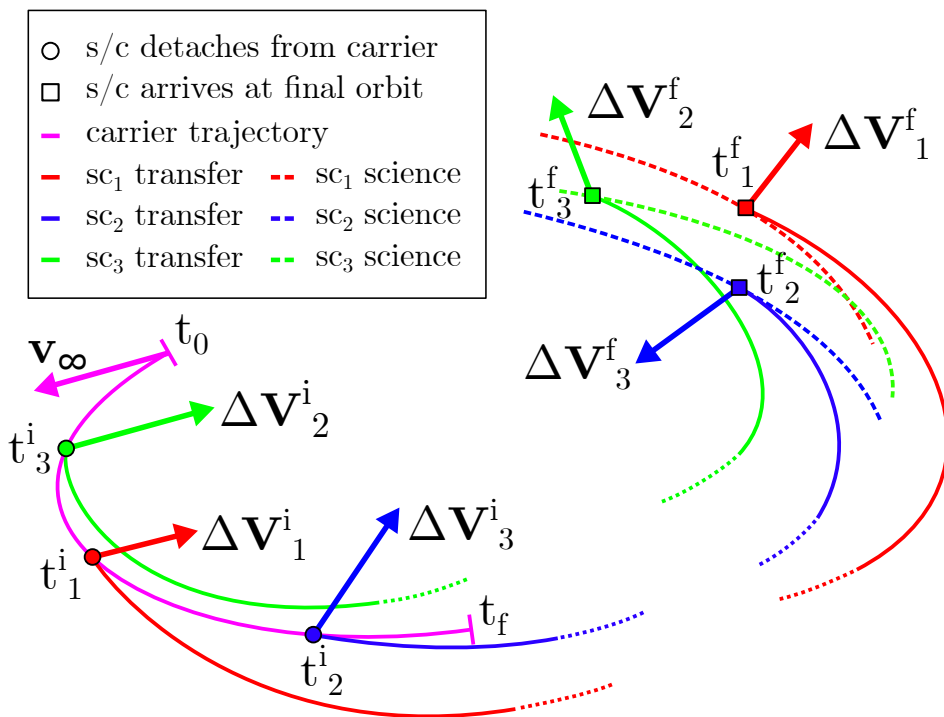


Figure 4.16: Diagram of the optimization process used for the second strategy.

# 5 | Results

The main objective of this work is to define a complete preliminary design of a trajectory transferring the cartwheel formation from Earth to an EDHO and analyse the main parameters that affect both the formation stability and the transfer. In this chapter, the results of the optimization problems and transfer strategies adopted to answer the research question are reported. In the first part regarding the science phase the results determining the stability of the formation are analysed by considering two cost functions,  $J_{\text{Length}}$  and  $J_{\text{Rate}}$ . The two approaches are compared using different initial displaced angles and nominal arm lengths to check if the requirements reported in Table 5.1 are satisfied and if one function is better than the other.

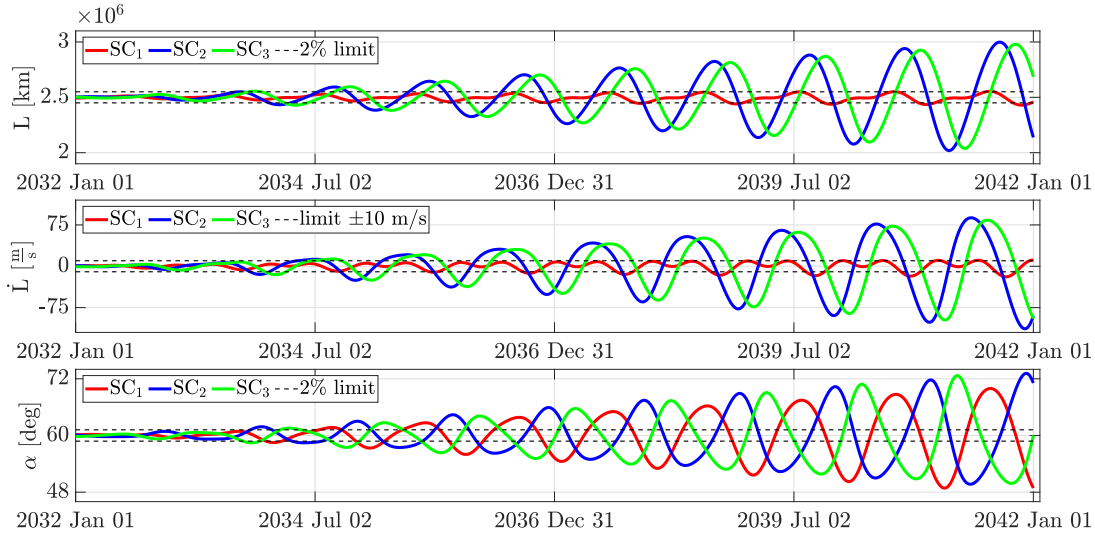
| L Range [km]                           | $\dot{L}$ Range [m/s] | $\alpha$ Range [deg] |
|--|-----------------------|----------------------|
| $[2.45 \times 10^6, 2.55 \times 10^6]$ | [-10, 10]             | [58.8, 61.2]         |

Table 5.1: Requirements on the geometry of the formation.

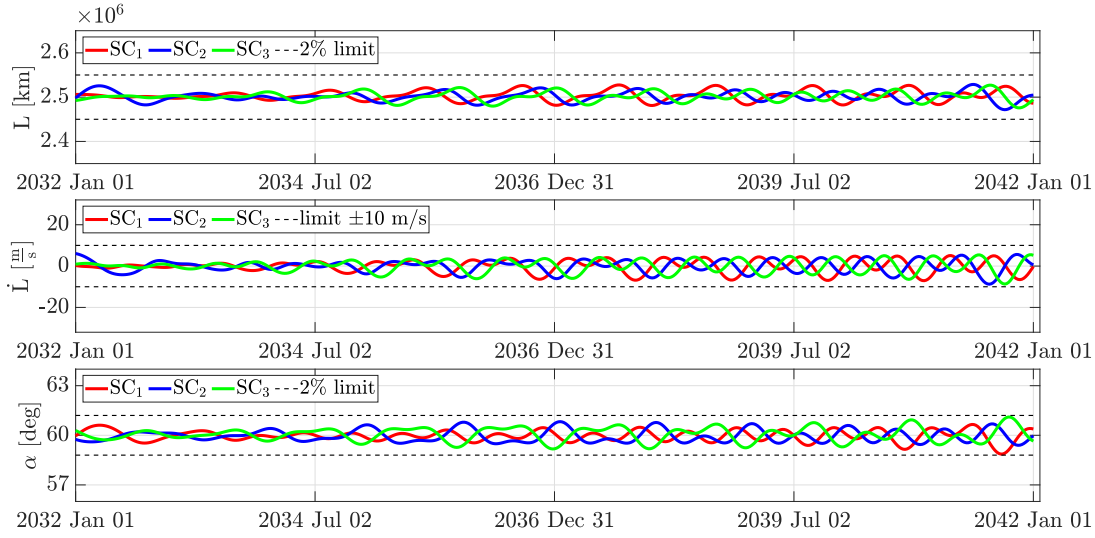
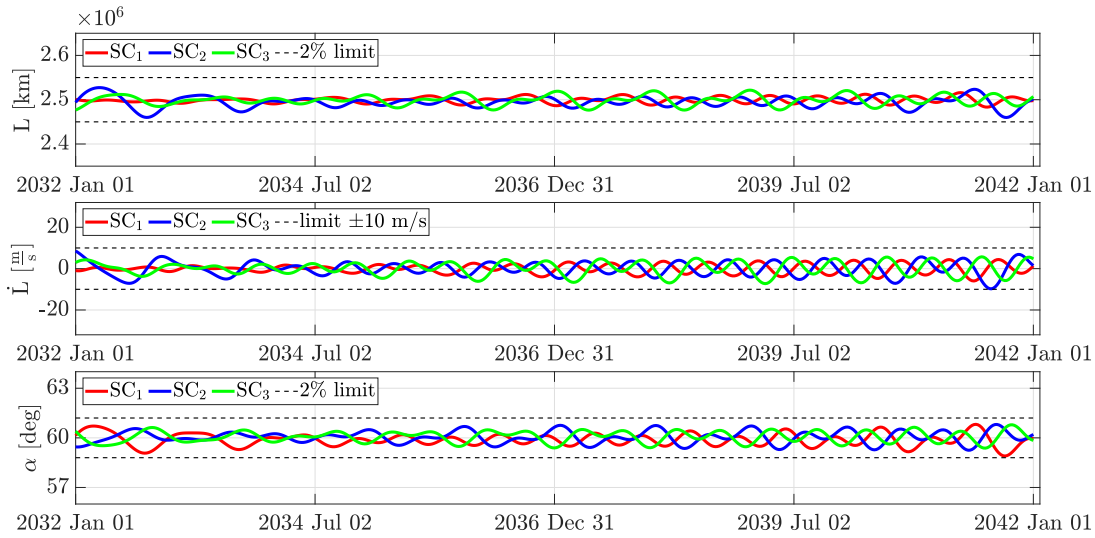
In the second part, the transfer strategies defined in Section 4.3 are analysed by fixing the structure of the formation, selecting the initial displacement angle and the arm length. After the evaluation of both strategies, their results will be assessed to understand which one obtained the best performance in terms of total  $\Delta V$  and maximum difference between the delta-Vs of each spacecraft.

## 5.1. Science Phase

The first step is to verify that by tuning the initial conditions defined by the orbital elements, the formation can be stabilized without station keeping manoeuvres for long periods of time, in this case 10 years. The test run presented in Fig. 4.5 refers to the geometry evolution of a formation defined by an initial displacement angle of  $-20^\circ$  and a nominal arm length of  $2.5e6$  km. The results of the optimization using the two cost functions with the same conditions are shown in Fig. 5.1; the *breathing* motion of the formation is lowered up to a point in which the geometry requirements are all satisfied.



(a) Not Optimized

(b) Optimized with  $J_{\text{Length}}$ (c) Optimized with  $J_{\text{Rate}}$ Figure 5.1: Formation with  $\theta_0 = -20^\circ$  and  $L = 2.5 \times 10^6$  km.

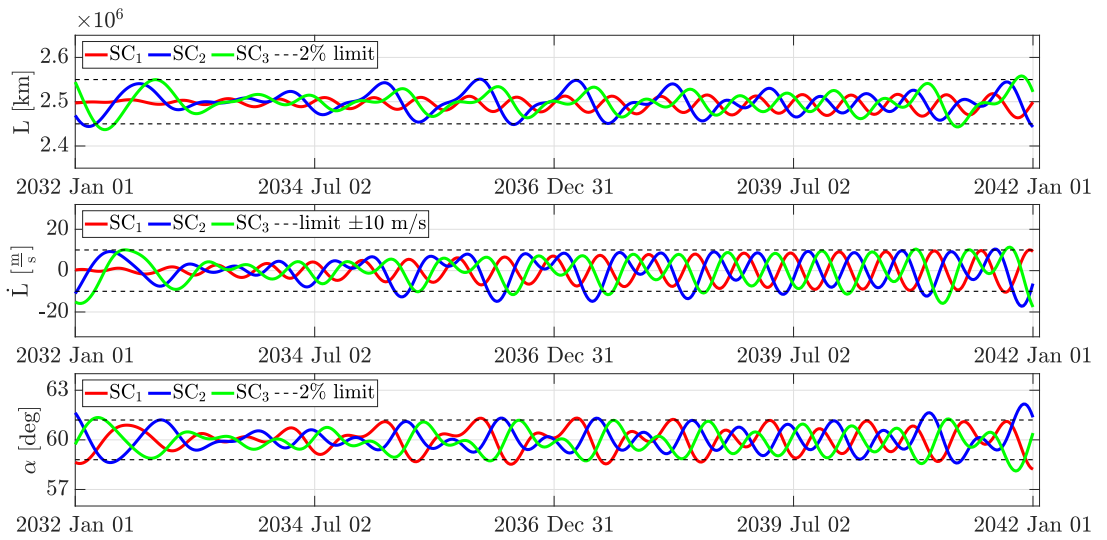
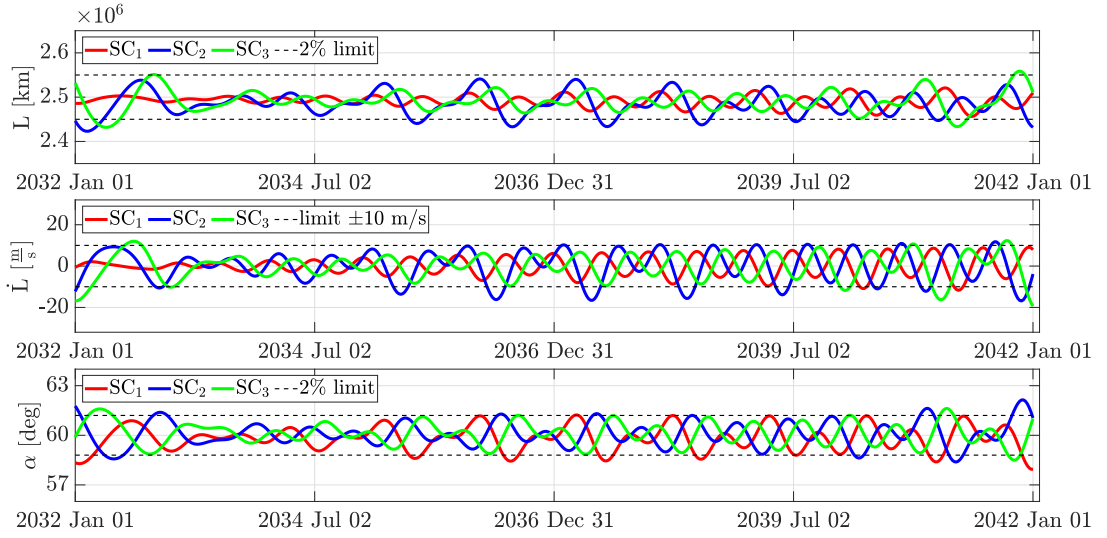
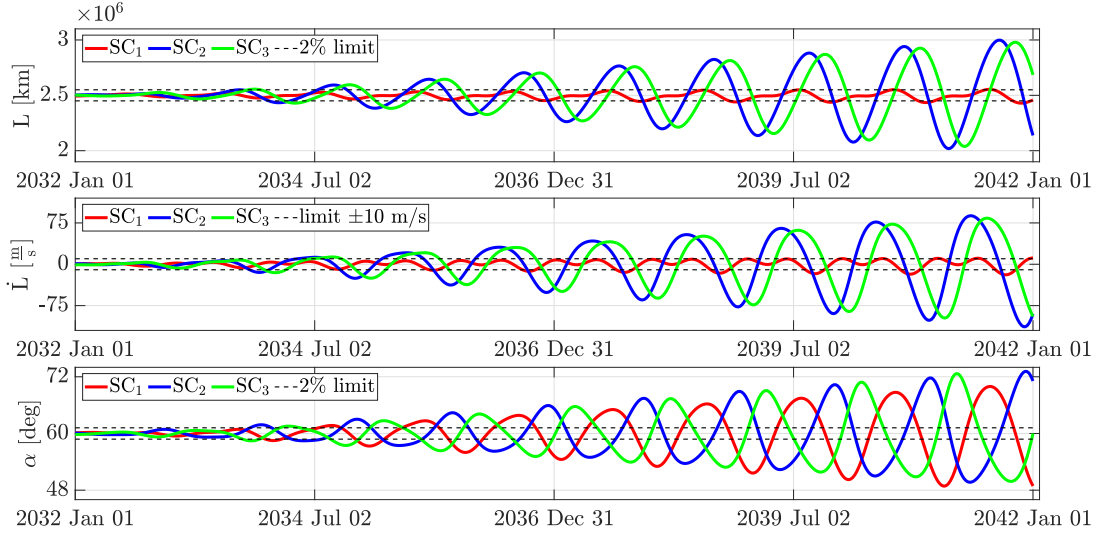


Figure 5.2: Formation with  $\theta_0 = 15^\circ$  and  $L = 2.5 \times 10^6$  km.

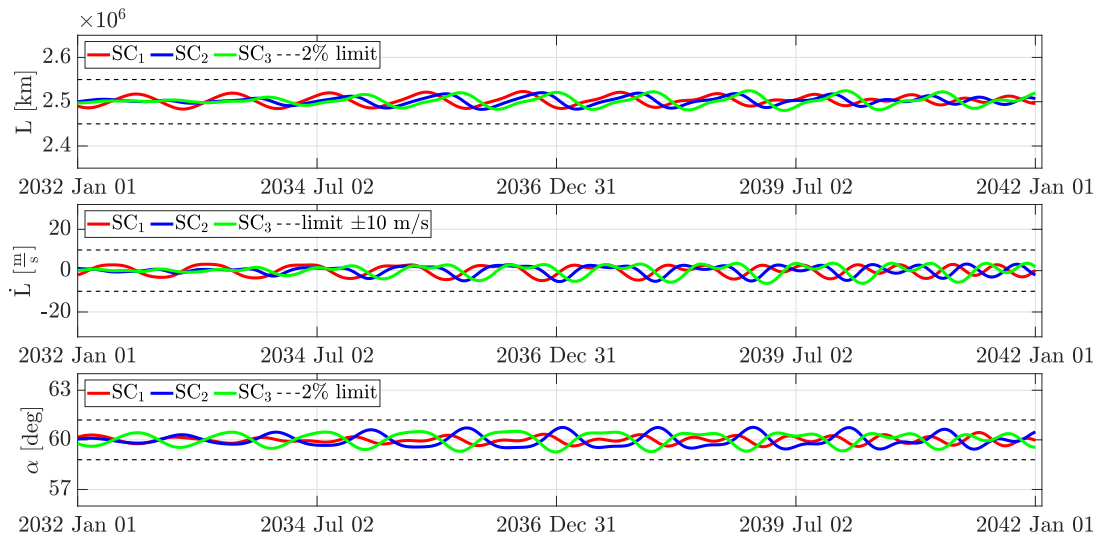
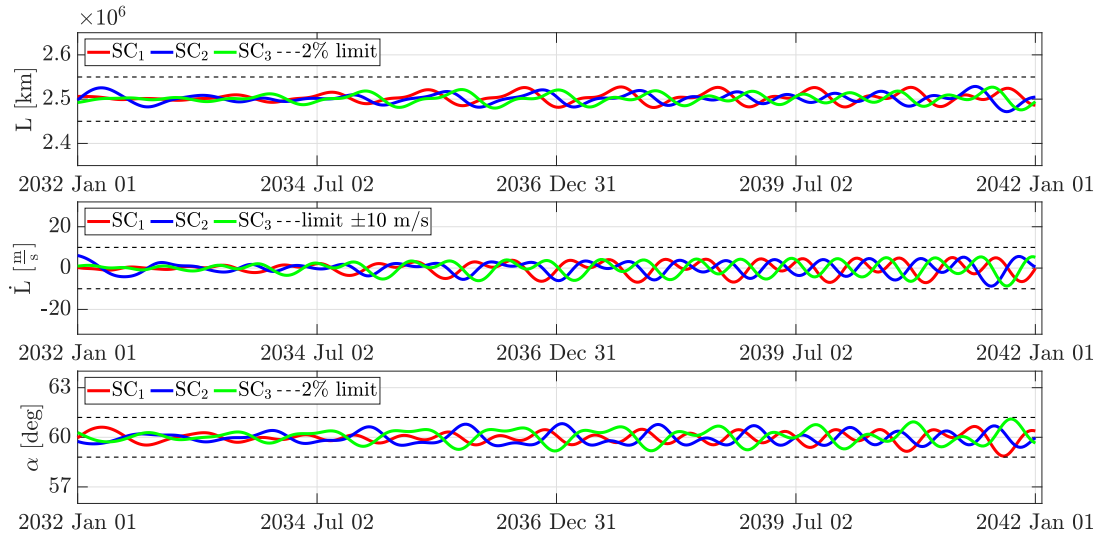
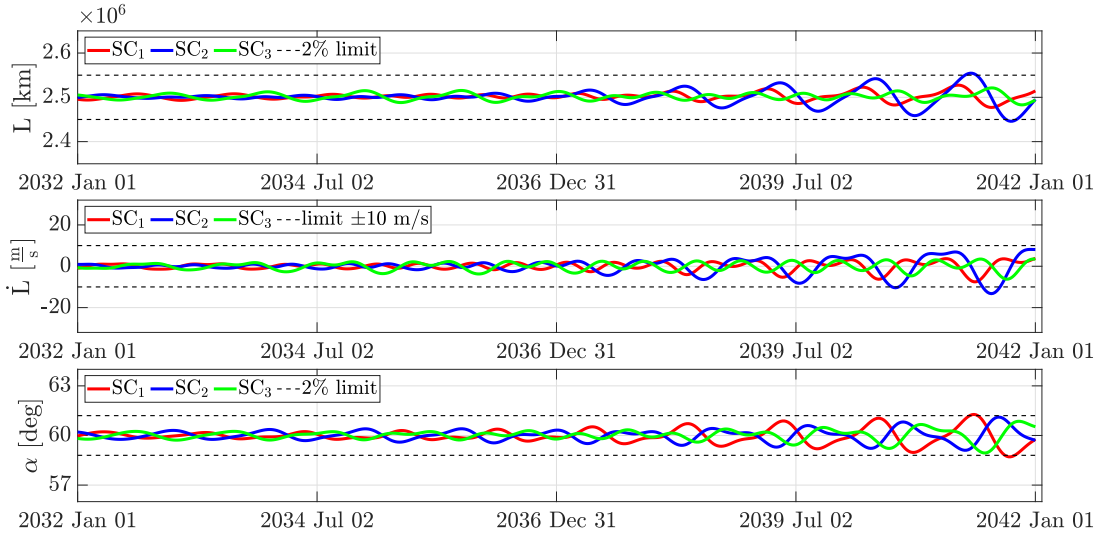


Figure 5.3: Formation with  $\theta_0 = -25^\circ$  and  $L = 2.5 \times 10^6$  km.

The geometry characteristics, instead of diverging in time as in the non-optimized case have a more uniform behaviour, verifying the success of the optimization process. The preliminary analysis in Section 4.1.1, studying leading and trailing configurations for a range of initial displacement angles from  $12^\circ$  to  $26^\circ$  (Fig. 4.6), shows a behaviour in the maximum deviation of the geometry parameter that can be categorized into three different levels: a highly perturbed formation for  $|\theta_0| < 16^\circ$ , where the geometry is still preserved but is not stable, a low perturbation environment for  $|\theta_0| > 24^\circ$ , in which there is no significant difference in the maximum deviation from the nominal conditions and an intermediate level, in which Earth's perturbations have a medium intensity. The analysis is repeated for initial angles in these ranges as reported in Fig. 5.2 and Fig. 5.3, respectively for  $\theta_0 = 15^\circ$  and  $\theta_0 = -25^\circ$ , to cover both leading and trailing configurations. As expected, the perturbation of Earth is too intense to have a formation satisfying the requirements even with the optimization. In the non optimized case the arm length ranges between  $2e6$  km and  $3e6$  km, the arm length rate between  $\pm 75$  m/s and the corner angle between  $48^\circ$  and  $72^\circ$ . The optimization manages to limit these large variations without bounding them within the imposed limits. It can be noticed that for the corner angle in the optimized cases the requirements are not met at the beginning and end of the time period considered. In case of a less perturbed environment ( $\theta_0 = -25^\circ$ ) even without optimization the parameters satisfied the bounds for the most of the time, exceeding these limits only in the last part of the propagation; in this situation, both functions manage to tune the initial orbital elements so that all requirements are satisfied.

To show the improvements due to the optimization for different  $\theta_0$ , the maximum and minimum value of  $L$ ,  $\dot{L}$  and  $\alpha$  are computed using optimized and non-optimized methods as shown in Fig. 5.4. For higher angles the action of the optimization is not that evident since the *breathing* motion is rather limited, while is quite the opposite for low angles where the optimization's results are remarkable, but the perturbations are too high to assure compliance with the requirements. The same figure is proposed focusing on the maximum deviation and the limits to analyse the behaviour of the two cost functions and understand which one produces the best results. As presented in Fig. 5.5,  $|\theta_0| = 15^\circ$  never complies with the requirements, while for most of the other cases the results are well bounded. Regarding the difference between the two cost functions, there is no clear trend that identifies the optimization problem which consistently produces the best results.

The investigation on the behaviour of  $J_{\text{Length}}$  and  $J_{\text{Rate}}$  continues by analysing the maximum variations of the geometrical parameters for different arm lengths with  $\theta_0 = -20^\circ$ . In this case the results are reported differently from Fig. 5.4 and only the difference between the maximum and minimum variation is reported for each value of  $L$ . The analysis is limited to more realistic values of arm length ranging from  $4e5$  km to  $5e6$  km, the latter

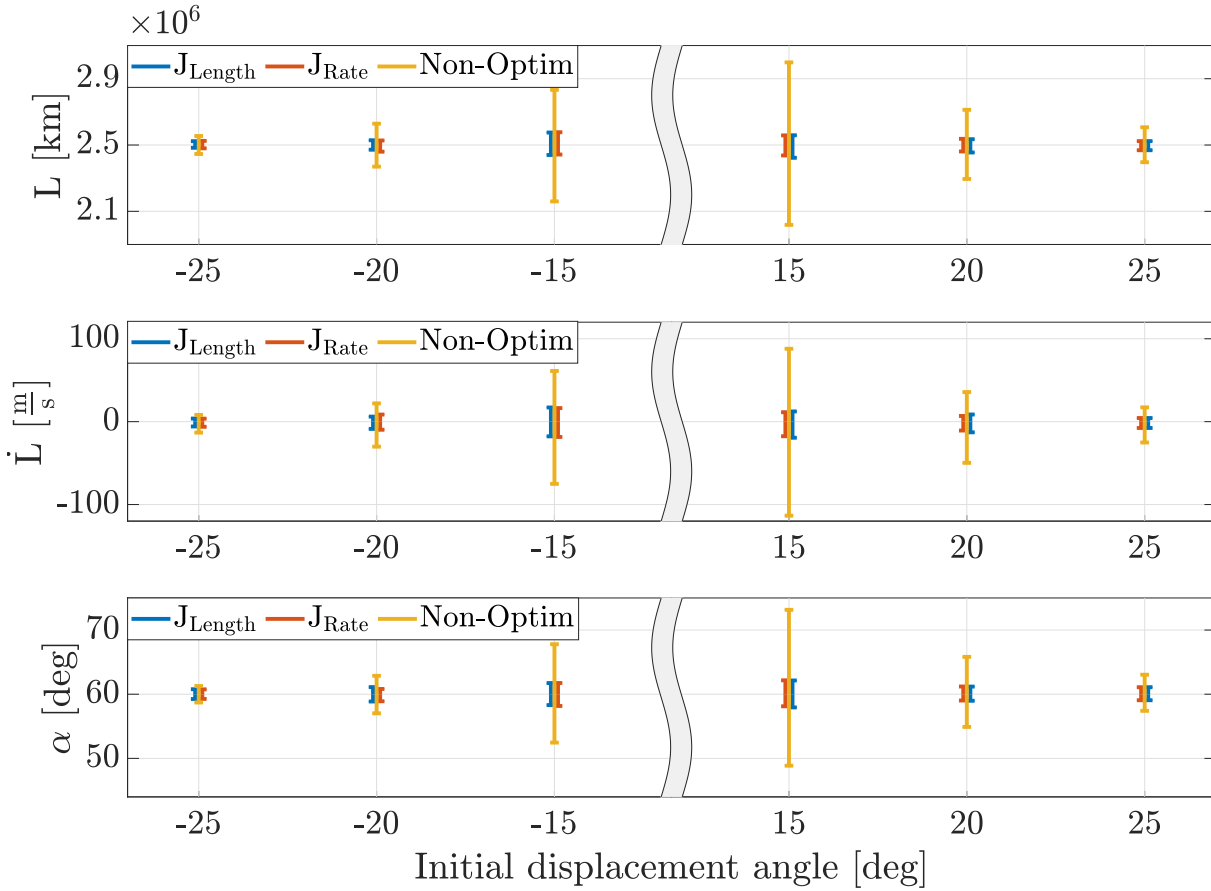


Figure 5.4: Maximum variation comparison between optimized and non-optimized solutions with respect to  $\theta_0$ .

being the nominal arm length of LISA selected in the early stages of the mission analysis. As shown in Fig. 5.6, both cost functions repeat the expected trend as in Fig. 4.7 with an increment in variations for  $L$  and  $\dot{L}$  for higher arm length and an initial decrement followed by a growth for the corner angle. The higher the value of the variation, the higher the *breathing* motion, meaning from this figure is possible to verify which optimization process performed worse. The cost function defined with the arm length obtains the best results for low inter-satellite distances up to  $2.5 \times 10^6$  km, point in which the two  $J$  have almost the same behaviour, with  $J_{Length}$  still being slightly better than  $J_{Rate}$ . For higher values of arm length the variations are approximately the same, but  $J_{Rate}$  achieves overall superior outcomes with respect to  $J_{Length}$ . From these results is possible to fully define the best cost function to optimize the science phase needed for the transfer; considering a nominal arm length of  $2.5 \times 10^6$  km and an initial displacement angle of  $-20^\circ$ , the cost function with the best results is  $J_{Length}$  and through this optimization is possible to create the OEM files needed to design of the transfer trajectory.

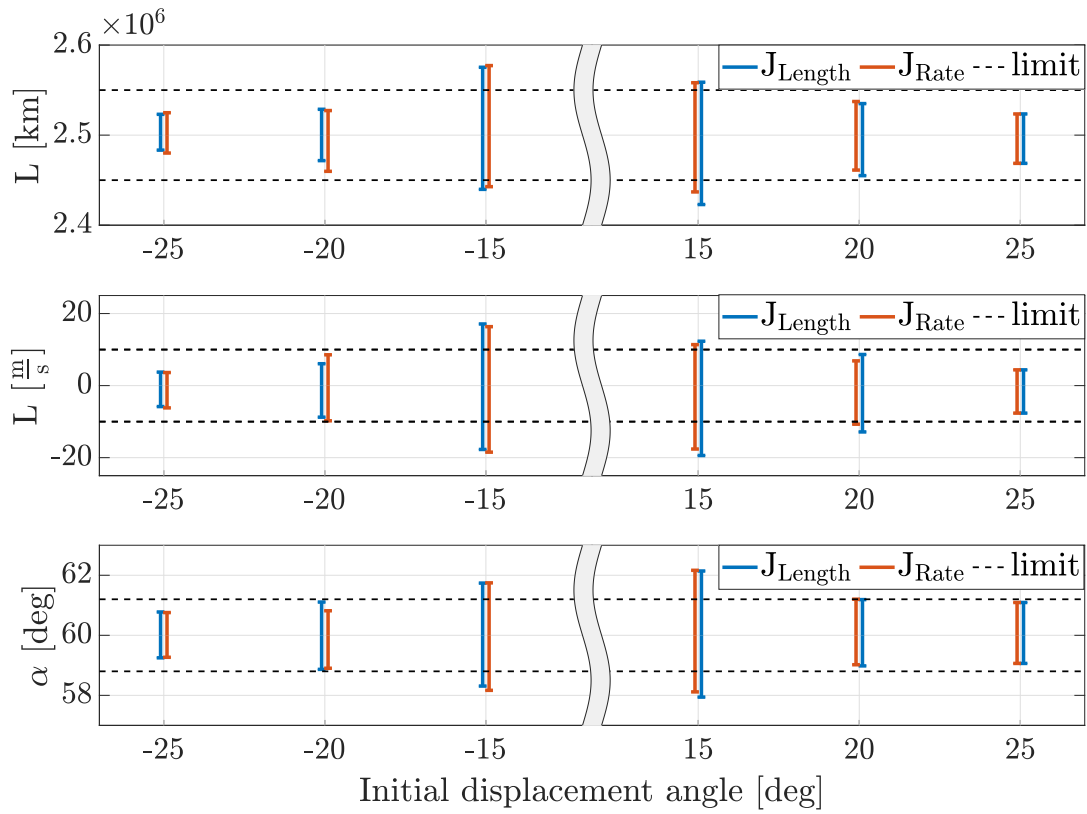


Figure 5.5: Maximum variation comparison between  $J_{\text{Length}}$  and  $J_{\text{Rate}}$  with respect to  $\theta_0$ .

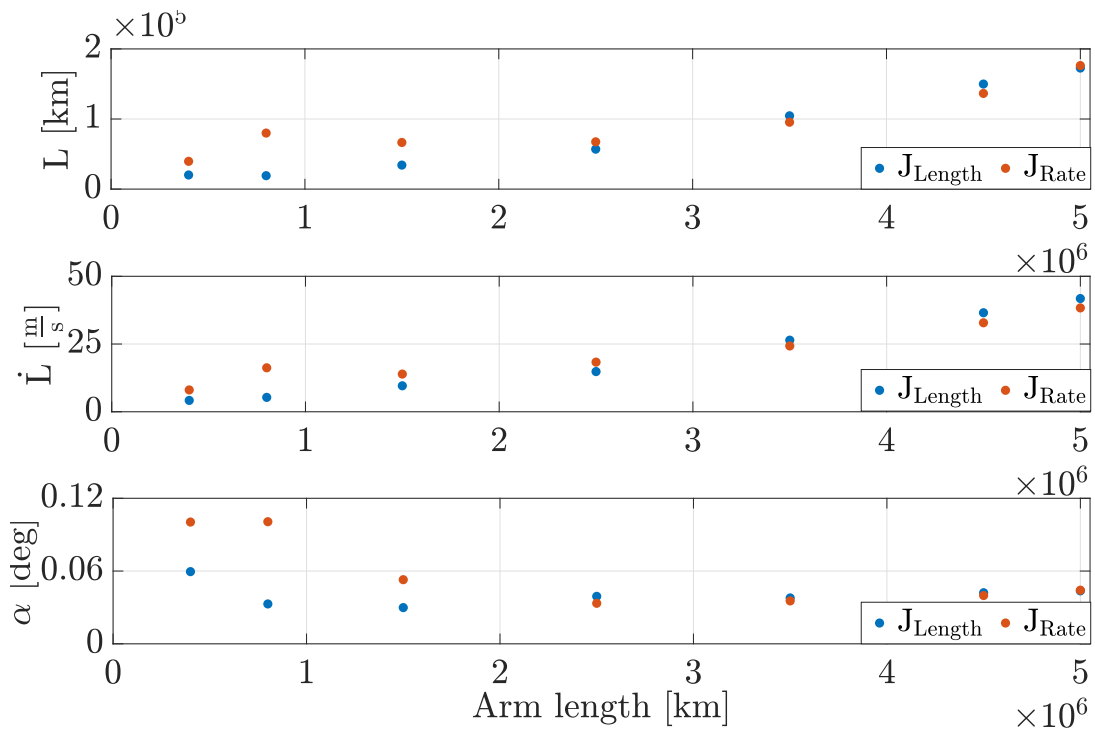


Figure 5.6: Maximum variation comparison between  $J_{\text{Length}}$  and  $J_{\text{Rate}}$  with respect to  $L$ .

## 5.2. Transfer Phase

The results obtained from the two transfer strategies are reported considering the same final orbits, fully defined in the optimization of the science phase. Only a single formation, the one with the same conditions as LISA, is investigated in order to compare the results with the one of LISA. It is fundamental to note that the results of the trajectory design of LISA reported in [22] come from a similar problem in terms of formation design, but with some key differences: the dynamic, that does not consider the SRP, the use of Solar Electric Propulsion (SEP), which set a range of acceptable Sun aspect angle (SAA), the presence of communications requirements, which determine a maximum Earth distance of 65e6 km and the departure epoch fixed in 2034, instead of 2031 as in the cases presented in this sections.

### 5.2.1. First Transfer Strategy

To solve the optimization problems presented in Section 4.3.1 it is necessary to choose a time for both the departure and arrival epochs which define the search space of the problem. Since the optimized science trajectories are computed from January 2032 onward, the arrival time is constrained to be after this date, meaning that the departure date can be found by subtracting the time of flight from the arrival date. The pork-chop plots in Fig. 4.9 represent the costs for a transfer from the mean Earth to the final science orbit; the time of flight for the optimal  $\Delta V$  is slightly lower than one year, meaning that considering the transfer without the hyperbolic leg 11 months is an acceptable guess. For the example reported in this section, the initial and final guessed dates are respectively

$$\begin{aligned} t_{i,\text{guess}} &= 2031-05-01T00:00:00 \\ t_{f,\text{guess}} &= 2032-04-01T00:00:00 \end{aligned}$$

with a window of two months centred in these epochs. Another parameter that needs to be defined is the magnitude of the infinite velocity which, with right ascension, declination and payload mass, imposes the performance of the launcher. The search space defined by the initial and final time and the  $v_\infty$  is the following:

$$\begin{aligned} t_{i,\text{range}} &= [2031-04-01T00:00:00, 2031-06-01T00:00:00] \\ t_{f,\text{range}} &= [2032-03-01T00:00:00, 2032-05-01T00:00:00] \\ v_{\infty,\text{range}} &= [300, 500] \text{ m/s} \end{aligned}$$

With the limits of the problem well defined is possible to solve Problem 1.1 obtaining the results reported in Table 5.2. The earliest date is the one relative to the third spacecraft, which is then taken as reference, meaning that Problem 1.2 needs to be solved only for

the other satellites as shown in Table 5.3. The departure date does not change excessively, meaning that the assumption made during the problem description regarding the similarity between the optimal releasing time and the time at which the satellite is on the SOI, can be considered valid.

|                       | $\Delta V$ [km/s] | $t_i$               | $t_f$               |
|-----------------------|-------------------|---------------------|---------------------|
| <b>SC<sub>1</sub></b> | 0.638             | 2031-05-22T12:07:20 | 2032-04-07T21:01:35 |
| <b>SC<sub>2</sub></b> | 0.652             | 2031-05-08T21:26:21 | 2032-03-19T16:22:39 |
| <b>SC<sub>3</sub></b> | 0.564             | 2031-04-27T18:05:45 | 2032-03-25T23:52:13 |

Table 5.2: Results obtained solving Problem 1.1.

|                       | $\Delta V$ [km/s] | $t_i$               | $t_f$               |
|-----------------------|-------------------|---------------------|---------------------|
| <b>SC<sub>1</sub></b> | 1.041             | 2031-05-28T09:50:58 | 2032-03-30T17:24:08 |
| <b>SC<sub>2</sub></b> | 0.837             | 2031-05-12T16:07:23 | 2032-03-28T09:35:08 |

Table 5.3: Results obtained solving Problem 1.2.

The total cost to transfer all three satellite is  $\Delta V = 2.442$  km/s, while the time of flight can be computed by defining the hyperbolic leg setting the perigee of the hyperbola at an altitude of 250 km. The resulting infinite velocity is 500 m/s and with such value the expected eccentricity is small, meaning that the escaping trajectory takes a non-negligible part of the transfer. In this example the total duration of the hyperbolic trajectory from the parking orbit to the SOI is about 7 days and the total times of flight for SC<sub>1</sub>, SC<sub>2</sub> and SC<sub>3</sub> are respectively 353, 334 and 340 days. As expected, the  $\Delta V$  of the satellite coupled with the carrier is much lower than the other; in this case  $\Delta V_3$  is half of  $\Delta V_1$  which makes the design and sizing of all the satellite system more complex and the management of the operational phase more challenging since a more cautious allocation of correcting manoeuvre must be considered. To conclude the analysis of the first strategy the entire trajectory transfer and part of the science phase are plotted in Fig 5.7. The carrier and the three satellites stowed in it leave Earth on a hyperbolic trajectory up to the SOI where the carrier and the third satellite continue on the same path. The other two satellites detach at an optimal time from the carrier and then perform an initial  $\Delta V$  manoeuvre that put them in the correct orbit to reach the final formation. All three satellites need a final manoeuvre to match the velocity of their respective final orbit, which in the figure are propagated only for one year to ease visually the reader.

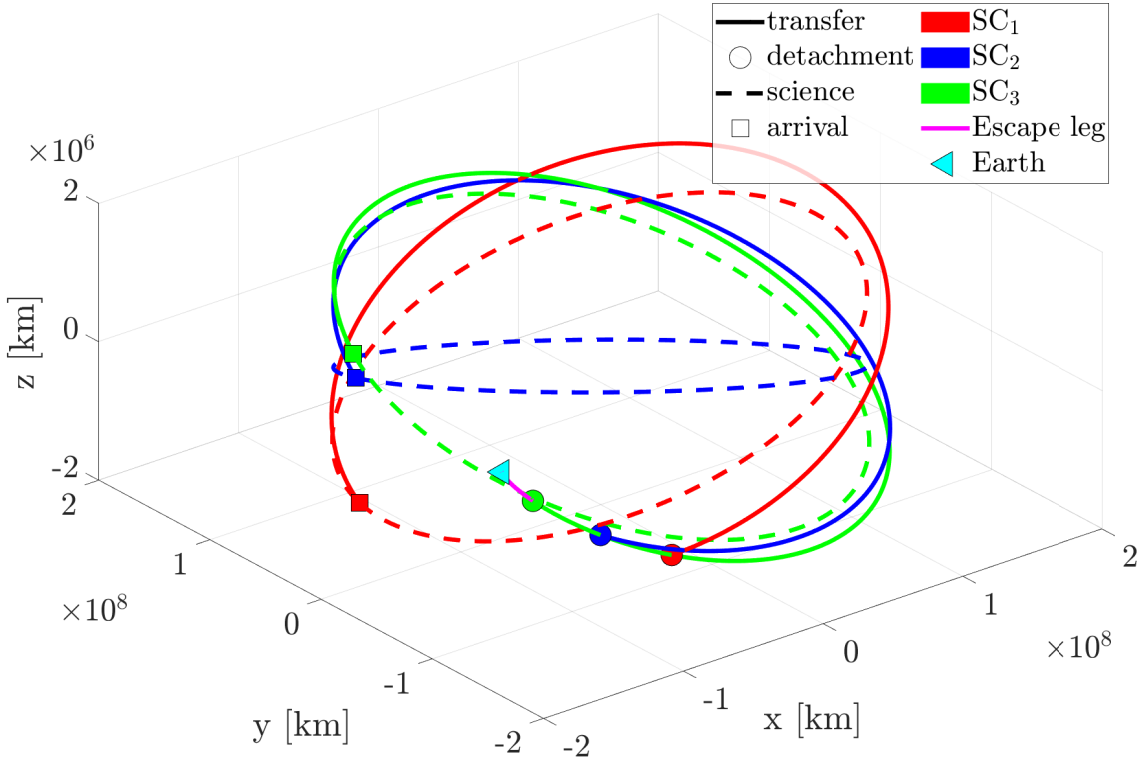


Figure 5.7: Transfer and science trajectories using the first strategy.

### 5.2.2. Second Transfer Strategy

The results of the second transfer strategy are presented as follows; firstly, a single optimization is shown as in the previous section, and then the optimization process is repeated for a whole year to obtain the best period to transfer the fleet. The first step to solve Problem 2 is to fix the time in which the carrier reaches the SOI, that for this example is:

$$t_0 = 2031-04-16T00:00:00$$

Then, the release times are selected after  $15 \div 20$  days from  $t_0$ , with a range of  $\pm 15$  days to define a search space of one month. By defining  $v_\infty$  with the same limits as the one in the first strategy the problem can be solved, obtaining the results reported in Table 5.4.

|                       | $\Delta V$ [km/s] | $t_i$               | $t_f$               |
|-----------------------|-------------------|---------------------|---------------------|
| <b>SC<sub>1</sub></b> | 0.965             | 2031-05-15T23:59:14 | 2032-03-31T21:51:33 |
| <b>SC<sub>2</sub></b> | 0.761             | 2031-05-01T04:51:10 | 2032-03-19T09:01:35 |
| <b>SC<sub>3</sub></b> | 0.735             | 2031-05-11T15:36:25 | 2032-04-07T00:47:22 |

Table 5.4: Results obtained solving Problem 2.

The total  $\Delta V$  of the transfer is 2.460 km/s which is slightly higher than the one obtained using the first strategy, recalling that in this case an additional initial  $\Delta V$  is expected. Regarding the difference in the delta-Vs of each satellite, the maximum difference is only 0.2 km/s, meaning that the new strategy defined to correct this performance difference does work. The optimized infinite velocity is not maximized as in the first strategy, since all three satellites depend on the initial infinite conditions. The newly defined optimization problem must seek an equilibrium that optimizes all releasing conditions simultaneously, while in the previous strategy the carrier optimization affected only one satellite. In this example the infinite velocity is

$$v_{\infty} = 424.3 \text{ m/s}$$

and the total times of flight from Earth to the final formation are 328, 330 and 339 days respectively for SC<sub>1</sub>, SC<sub>2</sub> and SC<sub>3</sub>, comparable with the results of the first strategy.

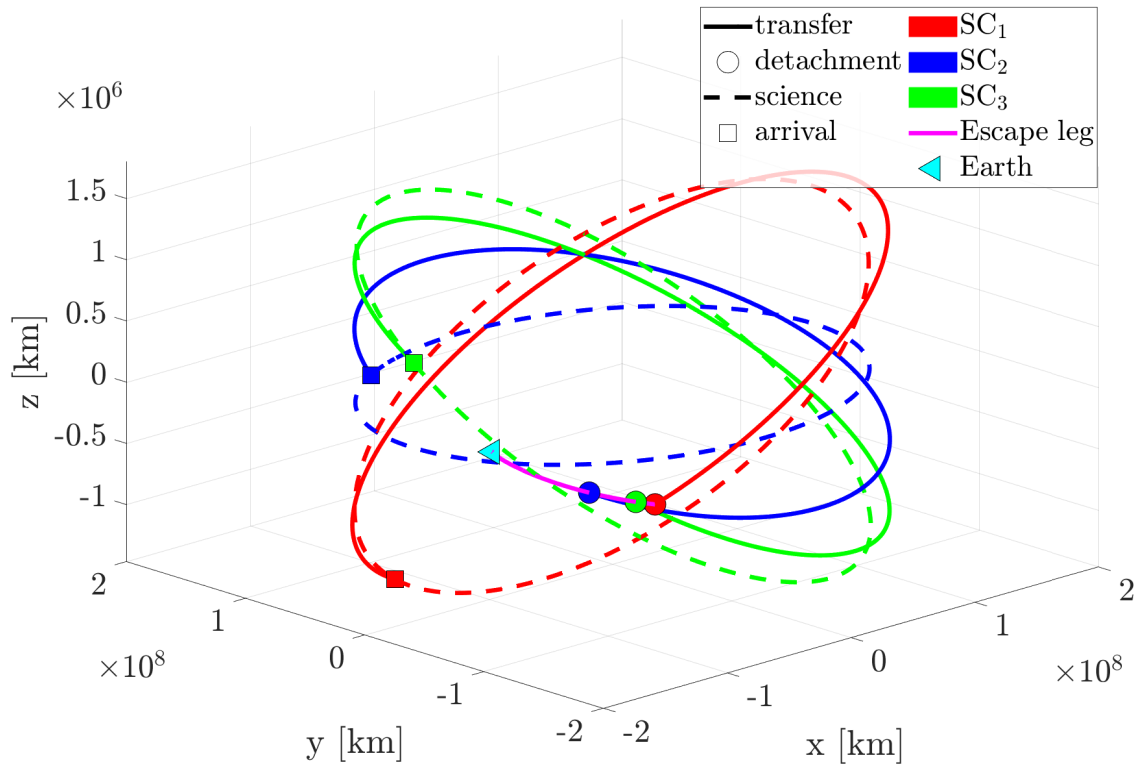


Figure 5.8: Transfer and science trajectories using the second strategy.

The complete trajectory is shown in Fig. 5.8; here the escape leg includes both the hyperbolic and the carrier trajectory which is propagated up to the final releasing epoch, coincident with SC<sub>1</sub>. Other than plotting the orbit is possible to check the behaviour of the geometry characteristics  $L$ ,  $\dot{L}$  and  $\alpha$  from  $t_0$  to one year into the science phase as shown in Fig. 5.9. Initially, all parameters are null since the satellites are still attached to the

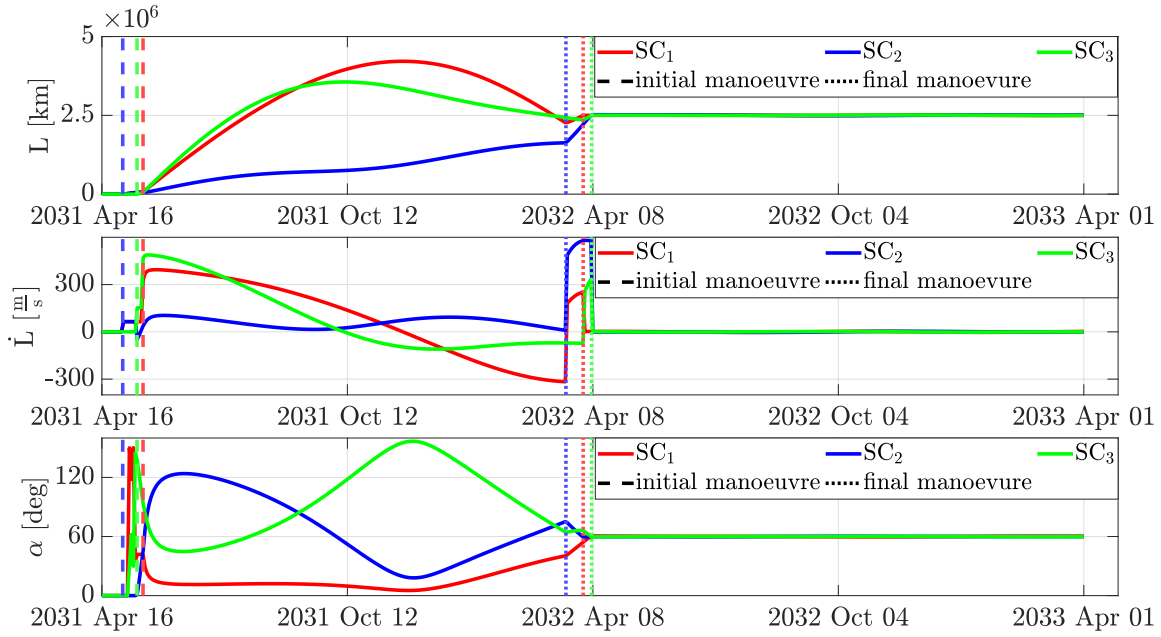


Figure 5.9: Geometry evolution during the transfer and part of the science phase.

carrier, then, with each impulsive initial manoeuvre, the formation starts to assume its form. The maximum value of the arm length is  $4.5e6$  km which is almost double the nominal value of  $2.5e6$  km, while the arm length rate and the corner angle have respectively a maximum of  $580$  m/s and  $150^\circ$ . In cases in which inter-satellite communications are needed also during the transfer, this could create problems on the communication system that should be sized on the geometry that the fleet assumes during the commissioning and not during the science phase.

To conclude this section, an in-depth analysis of this strategy is presented by analysing the behaviour of the  $\Delta V$  across an entire year. The time reference used to define the different delta-Vs is the epoch on which the carrier reaches the SOI,  $t_0$ ; for every new optimization,  $t_0$  is moved forward one month and the same happens to the initial and the final guessed times. The range selected to compute the additional optimization is one month since the allowed time window defined in the optimization problem is one month as well, meaning that the whole year is covered by the optimization process. Recalling that the scientific phase starts on January 2032 and the time of flight is on average 11 months, the first available date for  $t_0$  is 2031-02-16T00:00:00, while the last one is 2032-01-16T00:00:00. The results shown in Fig. 5.10 represent the total cost of the mission and the individual delta-Vs of each satellite for different departing epochs.

The cost of the mission varies along the year, but it is well bounded between  $2.5$  km/s and  $3.4$  km/s; by looking at the trend of  $\Delta V$ , it is possible to identify two local minima,

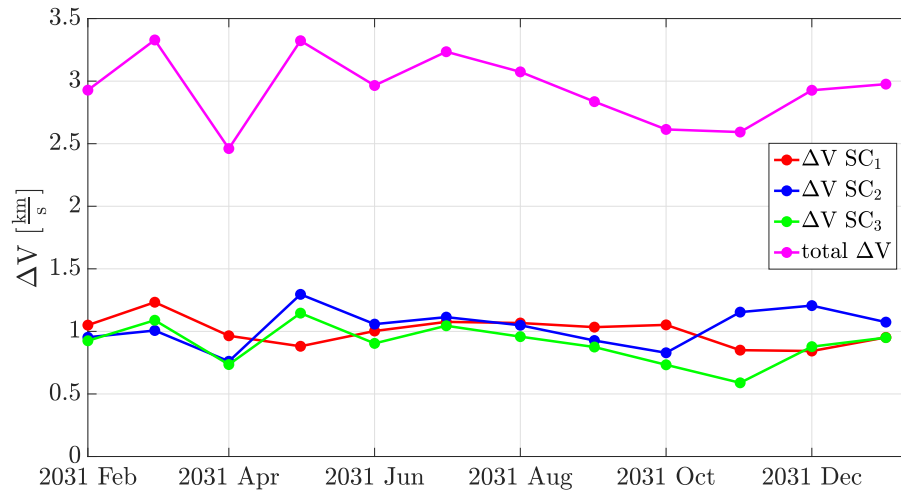
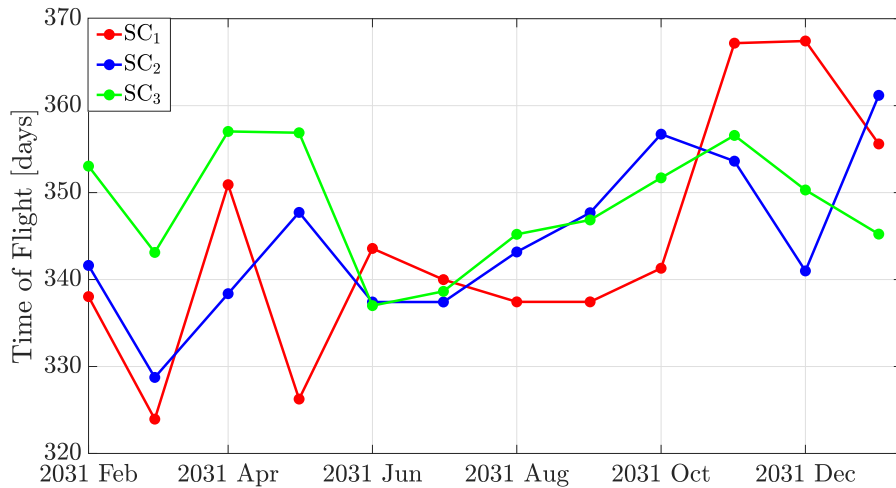
Figure 5.10:  $\Delta V$  trend for an entire year.

Figure 5.11: Time of flight variation over a one-year window.

one in April, the lowest, and one in October-November which is exactly what is expected by looking at the pork-chop plots in Fig. 4.9 for a trailing formation. Regarding the minimum and maximum difference between individual delta-Vs this analysis shows a varying behaviour with cases in which the three manoeuvres are almost identical and cases in which the costs are quite different. The two best and worst cases in this sense are obtained departing in July and November as reported in Table 5.5.

|                 | $\Delta V_1$ [km/s] | $\Delta V_2$ [km/s] | $\Delta V_3$ [km/s] | $\Delta V$ Difference [m/s] |
|-----------------|---------------------|---------------------|---------------------|-----------------------------|
| <b>July</b>     | 1.076               | 1.114               | 1.045               | 69                          |
| <b>November</b> | 0.850               | 1.154               | 0.589               | 556                         |

Table 5.5: Optimization results of July and November.

The minimum difference in  $\Delta V$  is just 69 m/s which is totally in agreement with the idea of using three identical spacecraft, but this comes at overall higher total cost of the mission equals to 3.236 km/s. From this analysis emerges the fact that this strategy does not prevent systematically results with major differences in  $\Delta V$ , but this phenomenon is largely limited due to the way the problem is constructed; in particular, by looking at the analysis over an entire year is possible to notice that the launch in November in which the difference in the delta-Vs is maximum is an isolate case. The last analysis deals with the transfer time elapsed from  $t_0$  to the final arrival time which does not consider the time spent on the hyperbolic leg of around 7 days; as shown in Fig. 5.11 the transfer duration for the different departure epochs ranges between 320 days and 370 days. From these results is clear that this approach can produce results as good as the first strategy with one less manoeuvre, but with better distribution of the costs between the three satellites of the fleet.

## 6 | Conclusions

The work developed in this thesis focuses on the preliminary mission design for a cartwheel formation in an EDHO, generalizing the dynamic environment in which this type of configuration was studied up to now. This final chapter outlines the main results and provides possible paths to future research.

The first step was to analyse the behaviour of the formation in a newly characterized dynamic environment which considered the presence of SRP to gain information on which parameters defining the formation affected its stability the most. The formation can be maintained stably without station keeping manoeuvre only for  $|\theta_0| \geq 20^\circ$ , threshold under which the Earth's perturbations are too intense to preserve a high-precision formation. The objective of designing a complete trajectory from Earth to the end of operation maintaining a stable formation and low transfer cost is reached as presented in Chapter 4. Regarding the stability, the proposed cost functions performed positively, achieving optimal performance in terms of minimization of the geometry's variation, highly limiting the *breathing* motion of the formation. The strategies proposed for the transfer succeeded in placing the satellites in their final heliocentric orbits with low-cost manoeuvres; the transfer considered only the main impulses, overlooking in first analysis small correction manoeuvres which are necessary for more refined mission design. The second strategy described in Section 4.3.2 obtained the overall best results considering the necessity of similar costs between the three satellites. The cartwheel formation used for the transfer analysis with  $\theta_0 = -20^\circ$  and  $L = 2.5e6$  km has been selected to be as close to LISA as possible and compare the outcomes. This thesis and the LISA mission analysis have some fundamental differences that are worth to be highlighted; LISA considered a SEP system from which additional constraints like limited SAA are derived, the selected departure epochs are in 2034, while in this work the launches are in 2031 and finally, LISA is not a mission in preliminary phases and there are additional restrictions on the transfer, such the ones on the communication system, imposing a maximum Earth's distance and elevation due to the limits of the High-Gain Antenna (HGA). Despite these differences, a fair comparison can be still carried out. The total  $\Delta V$  for LISA ranges between 2.0 and 3.0 km/s, while for this analysis the variation is limited between 2.5 and 3.4 km/s. This

distinction derives other than the previously discussed differences, from the discrepancy between the total time of flight of the transfer; for LISA this figure varies between 440 days and 540 days, while for the proposed strategy the transfer duration is much quicker ranging between 320 days and 370 days. In addition, the entirety of this thesis has been developed on GODOT to demonstrate and show the great potential of this software. In particular, the combination of GODOT and PyGMO makes the optimization, not only of the  $\Delta V$ s of the transfer but also of generic problems as the one needed for the stability of the formation, easy to implement and solve, due to the high compatibility of these two programs.

Despite the promising results, many future developments can improve and refine this type of solution starting from the selection of the escape trajectory. This thesis as a preliminary approach a direct injection toward the EDHO has been used considering the availability of a heavy-lift launch vehicle. Further improvements could consider smaller launchers defining different escape strategies; one possible example is the Lisa Pathfinder mission, launched on a Vega rocket toward the Lagrange point L1, in which an additional propulsion module performing six ARM was designed and added to the spacecraft. Other possible strategies consist in taking advantage of the lunar perturbations through Lunar Gravity Assist or exploiting low energy escape via the Sun-Earth Lagrange Points. Future work could also approach differently the solution to this problem without splitting the analysis into transfer and scientific parts. This would further complicate the problem since a single multi-objective optimization with multiple cost functions and constraints would be needed. Considering simultaneously the optimization of the initial conditions for the formation stabilization and the manoeuvres needed to transfer the fleet would produce a more general and complete solution to the cartwheel flying formation problem, to the detriment of a more complicated implementation.

## Bibliography

- [1] Chris Sabol, Rich Burns, and Craig A. McLaughlin. Satellite Formation Flying Design and Evolution. *Journal of Spacecraft and Rockets*, 38(2):270–278, 2001.
- [2] Jesse Leitner. Formation flying: The future of remote sensing from space. 02 2004.
- [3] C. Escoubet, Michael Fehringer, and Melvyn Goldstein. The Cluster mission. *Annales Geophysicae*, 19:1197–1200, 09 2001.
- [4] Byron D. Tapley. Gravity model determination from the GRACE mission. *The Journal of the Astronautical Sciences*, 56(3):273–285, Sep 2008.
- [5] R. Contreras, Luis Penin, V. Marco, Alexander Cropp, and Thibault Flinois. Proba-3 High precision Formation Flying in HEO. 02 2017.
- [6] Staffan Persson, Per Bodin, Eberhard Gill, Jon Harr, and John Jörgensen. PRISMA - An Autonomous Formation Flying Mission. 01 2006.
- [7] Staffan Persson, Simone D’Amico, and Jon Harr. Flight results from PRISMA Formation Flying and Rendezvous Demonstration Mission. *61st International Astronautical Congress 2010, IAC 2010*, 1, 01 2010.
- [8] Pau Amaro-Seoane et al. Laser Interferometer Space Antenna, 2017.
- [9] Steven P. Hughes. Preliminary Optimal Orbit Design for the Laser Interferometer Space Antenna (LISA). In *25th Annual AAS Guidance and Control Conference*, Breckenridge, CO, 2002.
- [10] Luciano Burderi, Andrea Sanna, Tiziana Di Salvo, Fabrizio Fiore, and Alessandro Riggio. ALBATROS & HERMES/SpIRIT: Probing Space-Time Quantum Foam and Hunting for Gravitational Wave Electromagnetic Counterparts. In *44th COSPAR Scientific Assembly. Held 16-24 July*, volume 44, page 1975, July 2022.
- [11] Kyle T. Alfriend, Srinivas R. Vadali, Pini Gurfil, Jonathan P. How, and Louis S. Breger. Chapter 4 - Nonlinear Models of Relative Dynamics. In Kyle T. Alfriend,

- Srinivas R. Vadali, Pini Gurfil, Jonathan P. How, and Louis S. Breger, editors, *Spacecraft Formation Flying*, pages 59–82. Butterworth-Heinemann, Oxford, 2010.
- [12] Simone D’Amico and Oliver Montenbruck. Proximity Operations of Formation-Flying Spacecraft Using an Eccentricity/Inclination Vector Separation. *Journal of Guidance, Control, and Dynamics*, 29, 05 2006.
- [13] Kyle T. Alfriend, Srinivas R. Vadali, Pini Gurfil, Jonathan P. How, and Louis S. Breger. Chapter 5 - Linear Equations of Relative Motion. In Kyle T. Alfriend, Srinivas R. Vadali, Pini Gurfil, Jonathan P. How, and Louis S. Breger, editors, *Spacecraft Formation Flying*, pages 83–121. Butterworth-Heinemann, Oxford, 2010.
- [14] Hanspeter Schaub. Relative Orbit Geometry Through Classical Orbit Element Differences. *Journal of Guidance, Control, and Dynamics*, 27(5):839–848, 2004.
- [15] Simone D’Amico. Autonomous Formation Flying in Low Earth Orbit. 2010.
- [16] Eric Joffre, Dave Wealthy, Ignacio Fernandez, Christian Trenkel, Philipp Voigt, Tobias Ziegler, and Waldemar Martens. LISA: Heliocentric formation design for the laser interferometer space antenna mission. *Advances in Space Research*, 67(11):3868–3879, 2021. Satellite Constellations and Formation Flying.
- [17] Arun Verma. An introduction to automatic differentiation. *Current Science*, 78(7), 04 2000.
- [18] Francesco Biscani and Dario Izzo. A parallel global multiobjective framework for optimization: pagmo. *Journal of Open Source Software*, 5(53):2338, 2020.
- [19] K Rajesh Nayak, S Koshti, S V Dhurandhar, and J-Y Vinet. On the minimum flexing of LISA’s arms. *Classical and Quantum Gravity*, 23(5):1763, feb 2006.
- [20] Eric Joffre, Waldemar Martens, Florian Renk, and Valerio Moro. Astrodynamics techniques for missions towards Earth-Trailing or Earth-Leading Heliocentric Orbits. 11 2018.
- [21] Andreas Rudolph. LISA Pathfinder Launch and Early Operations Phase - In-Orbit Experience. 05 2016.
- [22] Waldemar Martens and Eric Joffre. Trajectory Design for the ESA LISA Mission. *The Journal of the Astronautical Sciences*, 68(2):402–443, Jun 2021.